SEISMIC REFLECTION, REFRACTION, AND SURFACE WAVE STUDIES AT THE PROPOSED LOW-LEVEL RADIOACTIVE WASTE REPOSITORY, HUDSPETH COUNTY, TEXAS

by

Jeffrey G. Paine

Bureau of Economic Geology

W. L. Fisher, Director

The University of Texas at Austin

and

Kate C. Miller and Fa Hua

The University of Texas at El Paso

Final Report

Prepared for

Texas Low-Level Radioactive Waste Disposal Authority

under Interagency Contract Number IAC(92-93)-0910

October 1993

QAe7721

CONTENTS

Executive Summary 1
Introduction 4
Methods 4
Seismic Refraction 8
Seismic Reflection 10
Acquisition Geometry 10
Seismic Tests 10
Reflection Processing 13
Surface Wave 15
Borehole Velocity Survey 16
Results 16
Seismic Refraction 16
Spread LLRR1-2 18
Spread LLRR1-3 20
Spread LLRR1-4 23
Spread LLRR2 23
Spread LLRR3 26
Spread LLRR4 28
Seismic Reflection 29
Time-to-Depth Conversion 32
Line LLRL1 35
Line LLRL2 38
Line LLRL3 41
Line LLRL4 45
Integration of Borehole and Seismic Data 45

Surface Wave Analysis 50
Introduction 50
Data 51
Data Processing Procedures 55
Conclusions 60
Acknowledgments 66
References 67

Figures

1. Location of the Eagle Flat study area in West Texas 5
2. Borehole locations and depth to bedrock at Faskin Ranch 6
3. Map of Faskin Ranch refraction spreads LLRR1-2, LLRR1-3, LLRR1-4, LLRR2, LLRR3, and LLRR4 and nearby boreholes 9
4. Map of Faskin Ranch reflection lines LLRL1, LLRL2, LLRL3, and LLRL4 and nearby deep boreholes 11
5. End-shot field record LLRR6005 and interpreted record 17
6. First-break times, layer assignments, and layer velocities of refraction spread LLRR1-2 19
7. First-break times, layer assignments, and layer velocities of refraction spread LLRR1-3 21
8. First-break times, layer assignments, and layer velocities of refraction spread LLRR1-4 24
9. First-break times, layer assignments, and layer velocities of refraction spread LLRR2 25
10. First-break times, layer assignments, and layer velocities of refraction spread LLRR3 27
11. First-break times, layer assignments, and layer velocities of refraction spread LLRR4 29
12. Qualitative assessment of data quality along seismic reflection lines LLRL1, LLRL2, LLRL3, and LLRL4 31
13. Stacking velocities picked from CMP gathers 33

14. Combined field record from velocity survey at well YM-63 34
15. Velocity profile to 0.120 s derived from velocity survey of well YM-63 36
16. Faskin Ranch seismic reflection line LLRL1 37
17. Land surface and estimated bedrock elevations for reflection line LLRL1 39
18. Estimated basin-fill thickness beneath reflection line LLRL1 39
19. Faskin Ranch seismic reflection line LLRL2 40
20. Land surface and estimated bedrock elevations for reflection line LLRL2 42
21. Estimated basin-fill thickness beneath reflection line LLRL2 42
22. Faskin Ranch seismic reflection line LLRL3 43
23. Land surface and estimated bedrock elevations for reflection line LLRL3 44
24. Estimated basin-fill thickness beneath reflection line LLRL3 44
25. Faskin Ranch seismic reflection line LLRL4 46
26. Land surface and estimated bedrock elevations for reflection line LLRL4 47
27. Estimated basin-fill thickness beneath reflection line LLRL4 47
28. Depth-to-bedrock estimates from seismic reflection lines LLRL1, LLRL2, LLRL3, and LLRL4 48
29. Field records of surface wave experiment 52
30. Raw phase curves of 8-Hz records of westward-moving source 53
31. Raw phase curves of 40-Hz records of westward-moving source 54
32. Amplitude spectra of 8-Hz and 40-Hz phones at 50 m offset of the westward-moving source 56
33. Raw phase curves from a shot gather from reflection profile LLRL1 57
34. Amplitude spectrum of reflection data compared with surface-wave data from west-moving source 58
35. Example of Kalman filter fit 59
36. Phase velocity curves of 50-m center point, westward-moving source; 60-m center point, westward-moving source; and 70-m center point, westward-moving source 61
37. Curve fits for input to inversion: 50-m center point, westward-moving source; and 60-m center point, westward-moving source 62

38. Inversion models: 50-m center point, westward-moving source, and 60-m center point, westward-moving source 63

39. Fit of phase velocity predicted from inversion to original data: 50-m center point, westward-moving source, and 60-m center point, westward-moving source 64

Tables

1. Equipment, acquisition geometry, recording parameters, and field statistics of seismic surveys at Faskin Ranch 7

2. Processing steps, parameters, and purpose 14

3. Summary of reversed refraction data from Faskin Ranch 22

4. Velocity functions calculated from stacking velocity picks 35

EXECUTIVE SUMMARY

Seismic reflection, refraction, and surface wave methods were employed to characterize the shallow subsurface at the proposed low-level radioactive waste repository site located on Faskin Ranch about 5 mi (~8 km) southeast of Sierra Blanca, Texas. Reversed seismic refraction data were used to (1) determine near-surface compressional velocities for elevation datum corrections, (2) obtain preliminary velocity profiles for processing seismic reflection data, and (3) obtain depth-to-bedrock estimates. Seismic reflection data were used to determine basin geometry beneath the site, depth to bedrock, and internal basin-fill stratigraphy. Surface waves were analyzed to generate shear-wave-velocity models of the shallow subsurface.

Seismic reflection, refraction, and surface wave data were acquired in May and June of 1992 using a 500-lb (230-kg) accelerated weight drop seismic source, a 48-channel seismograph, and an acquisition crew supplied by the Bureau of Economic Geology (BEG) and The University of Texas at El Paso (UTEP). Refraction data were collected at six sites on Faskin Ranch and were processed and analyzed at BEG. Nearly 3.9 mi (6.2 km) of seismic reflection data were collected along one line oriented northwest-southeast across the site and three crossing lines oriented northeast-southwest. These data were processed and analyzed at both BEG and UTEP. Surface wave data were collected near the center of the proposed repository and were processed and analyzed at UTEP.

Three-layer velocity models provide adequate fits to refraction data from the five reversed and one unreversed spreads at Faskin Ranch. These models show increasing velocities with depth and consist of a thin, low-velocity surface layer, a thicker unit representing more consolidated basin fill, and a basal layer representing bedrock at most sites. The surface layer, which represents relatively dry and unconsolidated sediments, is 24 to 58 ft (7.2 to 17.7 m) thick and has compressional velocities ranging from 1243 to 1447 ft/s (379 to 441 m/s). This layer overlies layer 2, which is estimated to be 190 to 351 ft (58 to 107 m) thick and to have

velocities ranging from 3110 to 3629 ft/s (948 to 1106 m/s). These velocities are typical of unlithified basin-fill sediments. At five of the six refraction sites, the basal layer represents bedrock having seismic velocities greater than 6500 ft/s (>2000 m/s). Bedrock depths estimated from refraction data range from 220 to 384 ft (67 to 117 m) but are uncertain because of the limited offset range over which the bedrock refractor was observed. Layer 1 and layer 2 velocities were used successfully to make elevation datum corrections in the reflection lines and to make preliminary velocity corrections in seismic reflection data.

Reflection data quality ranged from good to poor across the site. The best data were collected along the long northwest-southeast line (LLRL1), where the interpreted bedrock reflector deepens from between 100 and 150 milliseconds (ms) of two-way time at the northwest end of the line to 250 to 300 ms at the southeast end. Several reflectors between 100 and 160 ms are interpreted within the basin-fill section on the southeast part of the line; these reflectors appear to onlap onto the bedrock surface. Time to depth conversions were made using velocity functions derived from the refraction and reflection surveys as well as from a vertical seismic profile acquired at well YM-63. Conversions of arrival times to depths of the interpreted bedrock reflector show that basin-fill thickness increases from about 200 ft (~60 m) at the northwest end of the line to 625 ft (190 m) near the southeast end of the line. Bedrock elevations decrease to the southeast from 4167 ft (1270 m) to 3691 ft (1125 m).

Reflection-data quality was not as high along the three crossing lines oriented northeast-southwest; consequently, interpretation of the bedrock reflector and depth-to-bedrock estimates are more uncertain along these lines. The interpreted bedrock reflector deepens to the northeast on all three lines, deepening from 100 ms to 200 ms on line LLRL2, from 125 to nearly 300 ms on line LLRL3, and from 100 to about 300 ms on line LLRL4. Estimated depths to bedrock increase to the northeast from 164 to 427 ft (50 to 130 m) on line LLRL2, from 246 to 656 ft (75 to 200 m) on line LLRL3, and from 328 to 656 ft (100 to 200 m) on line LLRL4. Reflectors are present within the basin fill, particularly on the east and northeast parts of the site where the basin fill thickens. On line LLRL3, basin-fill reflectors that are present between

100 and 250 ms terminate to the southwest as the bedrock reflector shallows. These basin-fill reflectors may mark the boundaries between distinct depositional units, or they may represent buried soil horizons having pedogenic carbonate accumulations.

Lithologic control of the seismic data is provided by boreholes YM-4, YM-5, YM-6, YM-17, YM-62, and YM-63. Seismic and borehole data indicate that the basin is deeper to the north and east than to the south and west. The southwest edge of the deepest part of the basin crosses the site in a northwest-southeast direction and intersects line LLRL1 between shotpoints 375 and 400, line LLRL3 between shotpoints 290 and 330, and line LLRL4 between shotpoints 194 and 228. Line LLRL2, south of the deep basin boundary, does not intersect it.

A feasibility study on using surface waves generated shear-wave-velocity models of Faskin Ranch. Calculated shear velocities generally increased with depth, from 591 to 1181 ft/s (180 to 360 m/s) near the surface to 2100 to 2789 ft/s (640 to 850 m/s) at depths of 131 to 164 ft (40 to 50 m). These velocity models, when combined with compressional velocity data determined from refraction surveys or downhole velocity surveys, can be used to characterize the physical properties of near-surface material at Faskin Ranch.

INTRODUCTION

The purpose of this study was to use shallow seismic methods to characterize the proposed low level radioactive waste repository site near Sierra Blanca, Texas. Seismic refraction methods were used to determine near-surface seismic velocities and estimate depth to bedrock at several sites on Faskin Ranch. Seismic reflection methods were used to determine basin geometry beneath the site, estimate the thickness of basin fill, and determine whether major stratigraphic discontinuities exist within the basin fill. Measurements of seismic surface waves were used to determine the shear-wave velocity of near-surface sediments at the site.

The site of the proposed repository lies on Faskin Ranch in the Eagle Flat study area about 5 mi (~8 km) southeast of Sierra Blanca in Hudspeth County, Texas (fig. 1). Most of the seismic work was completed on the site footprint, which lies on the part of the ranch between Interstate Highway 10 and the Southern Pacific Railway (fig. 2). The site lies in a late Cenozoic extensional basin that is partly filled by late Tertiary and Quaternary alluvial, colluvial, and eolian sediments having textures ranging from gravel to clay. Cores obtained from boreholes on the site (fig. 2) indicate that (1) the dominant texture is silty clay to sandy silt, (2) buried calcic soil horizons are present within the basin fill, and (3) the basin is floored by Cretaceous bedrock. The basin-fill sediments are dry, loose to indurated, and tens to hundreds of feet thick. The water table lies 650 to 1000 ft (200 to 300 m) below the surface at the site.

METHODS

Shallow seismic refraction, reflection, and surface wave techniques were used in this study. The seismic source chosen for the work is the Bison EWG-III, a noninvasive, stackable 500-lb (230-kg) accelerated weight drop unit (table 1). Data were acquired for all three techniques on a 48 channel Bison 9048 seismograph, transferred to a Macintosh computer, and processed using Seismic Processing Workshop (SPW) on a Macintosh and ProMAX on an IBM computer.

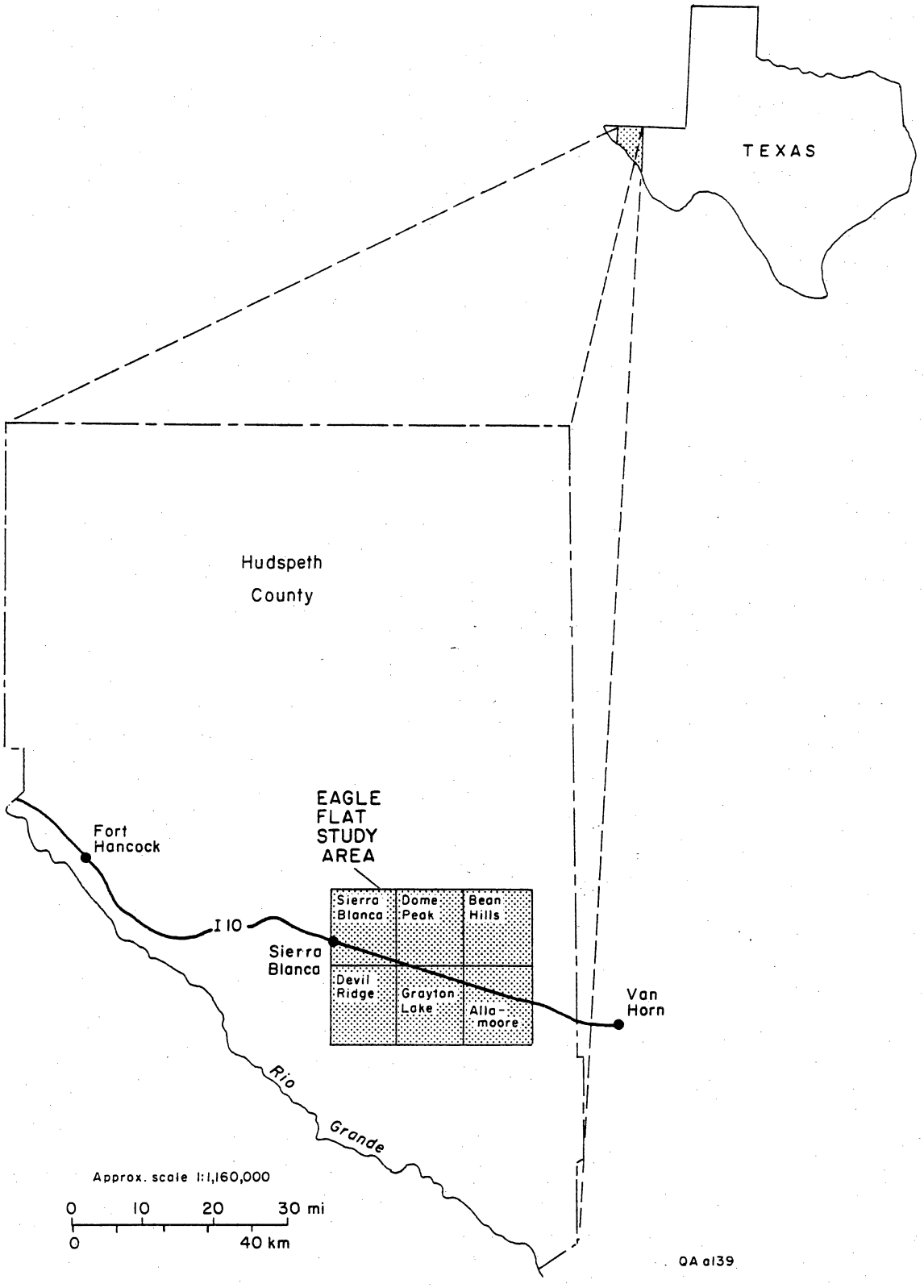

Figure 1. Location of the Eagle Flat study area in West Texas.

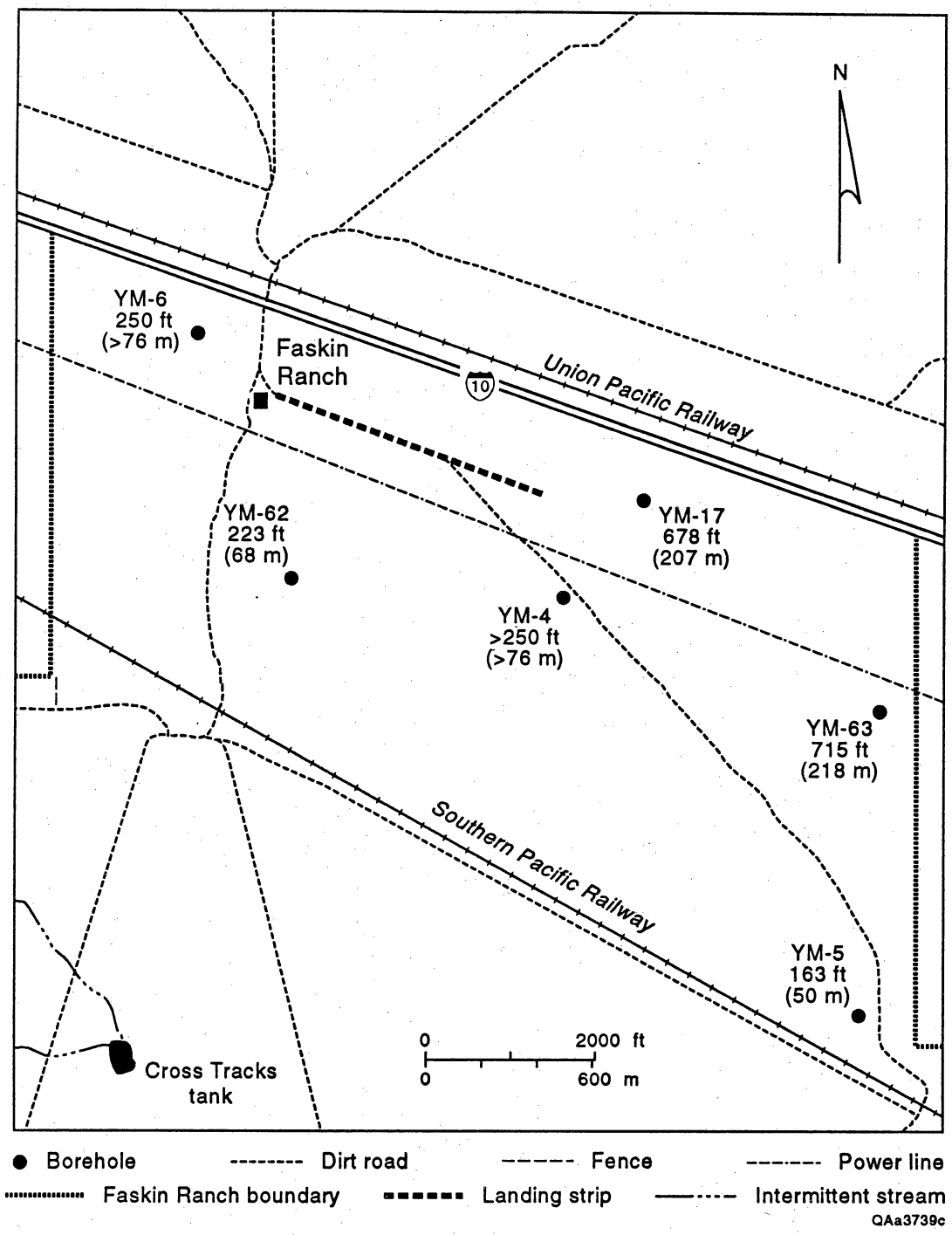

Figure 2. Borehole locations and depth to bedrock at Faskin Ranch.

Table 1. Equipment, acquisition geometry, recording parameters, and field statistics of seismic surface wave, refraction, and reflection surveys at Faskin Ranch.

	Surface wave	Refraction	Reflection			
			LLFR1	LLFR2	LLFR3	LLFR4
Equipment						
Seismic source	Bison EWG III	Bison EWG III	Bison EWG III	Bison EWG III	Bison EWG III	Bison EWG III
Geophones	8 Hz and 40 Hz	40 Hz	40 Hz	40 Hz	40 Hz	40 Hz
Seismograph	Bison 9048	Bison 9048	Bison 9048	Bison 9048	Bison 9048	Bison 9048
Geometry						
Source offset	10 to 310 m	2.5 to 352.5 m	15 m	15 m	15 m	20 m
Source spacing	10 m	117.5 m	5 m	3 m	3 m	5 m
Spread length	–	235 m	235 m	141 m	141 m	115 m; 115 m
Source–receiver geometry	–	–	End on	End on	End on	Split
Geophones in array	12 (8 Hz); 1 (40 Hz)	1	1	1	1	1
Geophone spacing	podded	5 m	5 m	3 m	3 m	5 m
Recording parameters						
Recording channels	3	48	48	48	48	48
Sample interval	0.002 s	0.001 s	0.001 s	0.001 s	0.001 s	0.001 s
Record length	2 s	1 s	1 s	1 s	1 s	1 s
Analog low-cut filter	4 Hz	4 Hz	16 Hz	16 Hz	32 Hz	16 Hz
Analog high-cut filter	250 Hz	500 Hz	250 or 500 Hz	250 Hz	250 or 500 Hz	500 Hz
Statistics						
Line length	–	–	2,575 m	948 m	1,452 m	1,180 m
Shots per shotpoint	1 to 4	1 to 12	4	4	4	4
Date acquired	6/7/92	LLRR1-2: 5/27/92 LLRR1-3: 5/25/92 LLRR1-4: 5/26/92 LLRR2: 5/22/92 LLRR3: 5/25/92 LLRR4: 5/26/92	6/5 to 6/6/92	5/22 and 5/24/92	6/3 to 6/4/92	6/2 to 6/3/93

Acquisition personnel included a survey crew of two who operated an optical theodolite and metric staff and surveyed shotpoint and geophone locations and a seismic crew of three who operated the seismograph, moved the source from shotpoint to shotpoint, fired the source, and moved and installed cables and geophones. Crewmembers were supplied by the Bureau of Economic Geology (BEG) and the Geoscience Department of the University of Texas at El Paso (UTEP). All data were acquired in May and June 1992. Because the acquisition system uses metric units, discussion of acquisition parameters and geophysical properties is in metric units. English system equivalents are used, along with their metric equivalents, in discussions of calculated depths, elevations, and on-the-ground distances.

Seismic Refraction

Refraction data were collected at six sites on Faskin Ranch (fig. 3). Three reversed spreads (LLRR2, LLRR3, and LLRR4) were oriented northeast-southwest; two reversed spreads (LLRR1-2 and LLRL1-4) and one unreversed spread (LLRL1-3) were oriented northwest-southeast. The geophone spread consisted of 48 40-Hz geophones spaced at 16.4 ft (5 m) intervals along a surveyed line 771 ft (235 m) long (table 1). The weight-drop source was fired at five sites spaced 386 ft (117.5 m) apart: one at the center of the geophone spread, one at each end of the spread, and one 386 ft (117.5 m) beyond each end of the spread. Source to receiver offsets ranged from 8.2 to 1156.5 ft (2.5 to 352.5 m). The number of shots at each shotpoint increased from 1 at the center of the geophone spread to a maximum of 12 when the source was farthest from the geophones. Data were recorded on the seismograph at a 1-ms sample interval, a 1-s record length, and a 4-Hz low-cut filter, the lowest possible setting (table 1).

After the refraction data were transferred to a Macintosh computer, first arrivals were picked using SPW and then exported to a spreadsheet program in which layer assignments and apparent velocity measurements were made and zero-offset intercept times were calculated for

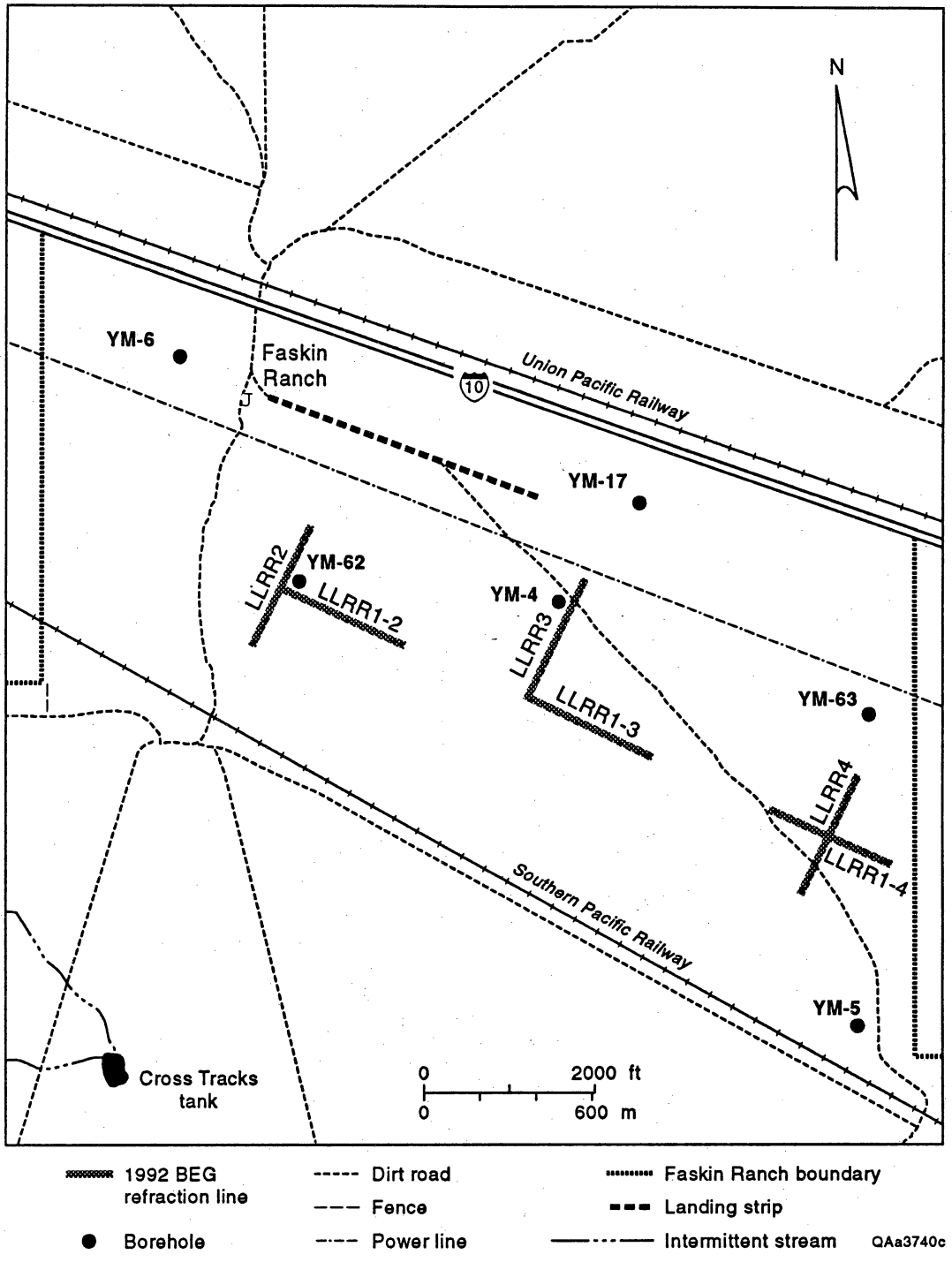

Figure 3. Map of Faskin Ranch refraction spreads LLRR1-2, LLRR1-3, LLRR1-4, LLRR2, LLRR3, and LLRR4 and nearby deep boreholes.

critically refracted arrivals from layers 2 and 3. True velocities, layer thicknesses, and apparent-dip angles were calculated using the slope-intercept method (Palmer, 1986; Milsom, 1989).

Seismic Reflection

Acquisition Geometry

Four shallow seismic reflection lines were acquired on Faskin Ranch (fig. 4) using the common depth point method adapted to the shallow subsurface (Mayne, 1962; Steeples and Miller, 1990). These lines cover a total distance of 3.9 mi (6.1 km) and include three short lines oriented northeast-southwest (LLRL2, LLRL3, and LLRL4) and one longer crossing line oriented northwest-southeast (LLRL1). Acquisition geometry varied from line to line (table 1); shorter geometries were used on lines LLRL2, LLRL3, and LLRL4 because bedrock depths were anticipated to be 150 to 300 ft (46 to 91 m) from completed boreholes YM-4, YM-5, and YM-6. When analysis of refraction data and continued drilling revealed potentially deeper bedrock depths, a longer geometry was used for line LLRL1, the last line collected.

Source–receiver geometries were asymmetric (end on) for lines LLRL1, LLRL2, and LLRL3, with the weight drop source trailing a 48-geophone spread (table 1). Line LLRL4 was collected using a symmetric split-spread geometry. In this configuration, the source lay between two 24-geophone spreads. Single 40-Hz geophones were used at each geophone location on all lines. Shotpoints and geophone locations were surveyed at 9.8-ft (3-m) intervals on lines LLRL2 and LLRL3 and at 16.4-ft (5-m) intervals on lines LLRL1 and LLRL4. Shot and geophone spacings were equal for each of the lines, resulting in 24-fold reflection data.

Seismic Tests

Seismic tests performed at the site included noise, walkaway, filter, and stacking tests. During the noise and walkaway tests, the seismograph was connected to a spread of

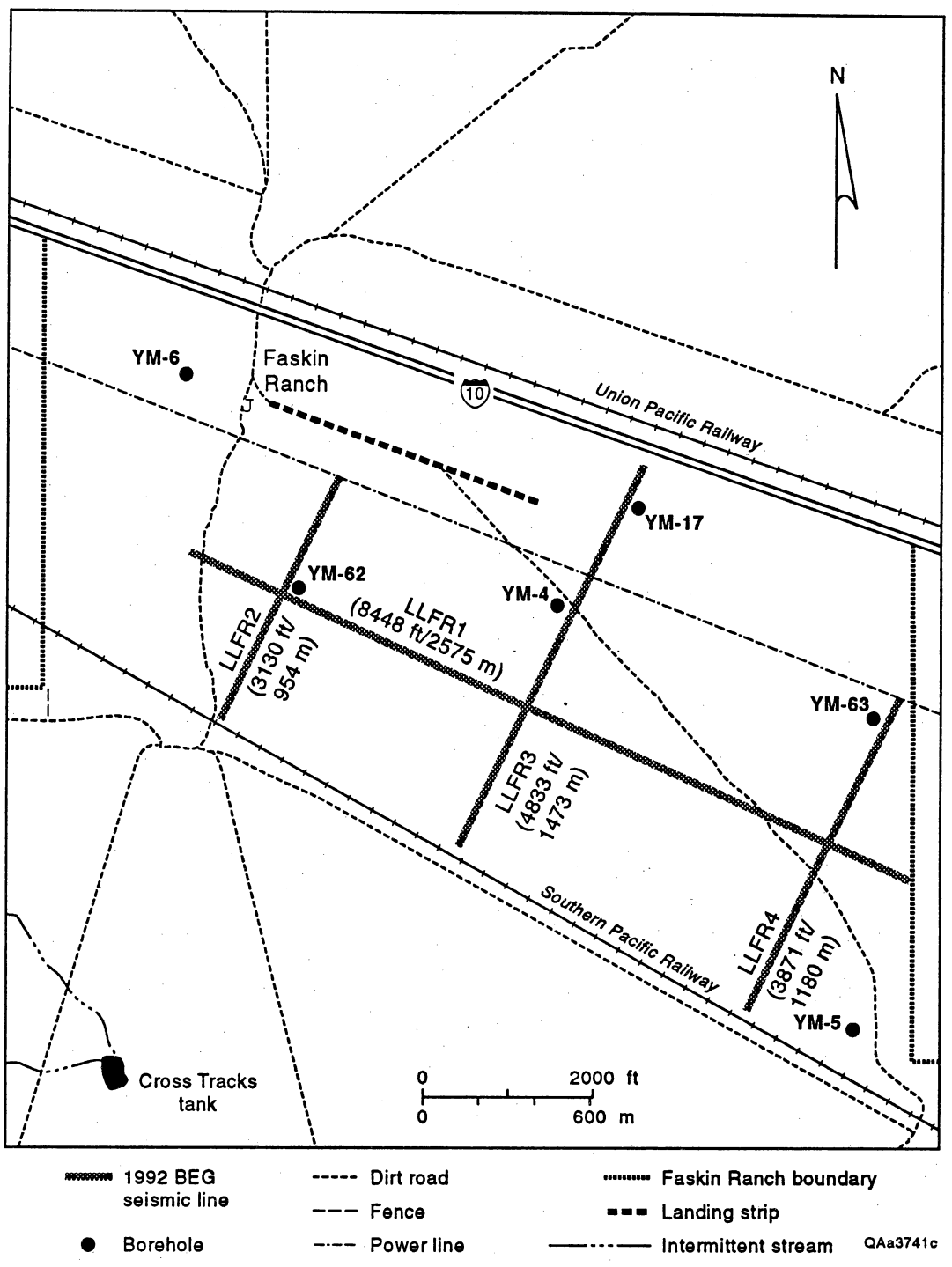

Figure 4. Map of Faskin Ranch reflection lines LLRL1, LLRL2, LLRL3, and LLRL4 and nearby deep boreholes.

48 geophones spaced at 3.3-ft (1-m) intervals. During the noise test, the seismograph recorded background seismic noise without a source being activated. This test and observations made during the remainder of the survey revealed that wind, passing trains, traffic on Interstate Highway 10, and overhead power lines were sources of noise. Although wind noise was severe at times, it was largely unavoidable. Highway traffic noise was a problem only near the north end of line LLRL3. One power line that crosses the site (fig. 4) reduced data quality along a small part of line LLRL3 and near the north ends of lines LLRL2 and LLRL4. Train noise, though severe at times, was easily avoided by not recording until the train had left the area.

Walkaway tests were performed to determine the optimum source–receiver offset range in the reflection survey. The source was fired at successively greater distances from the geophone spread after the low-cut filter had been calibrated to its lowest setting. The optimum offset range begins as close to the source as possible, but not so close that the nearest geophones become saturated by high-amplitude surface waves or source-related noise. The farthest offset should be equal to or greater than the depth of the deepest target. Based on these tests, a 49.2-ft (15-m) minimum source–receiver offset and a 9.8-ft (3-m) geophone spacing were chosen. Maximum source–receiver offset was thus 462.6 ft (141 m).

Filter tests were conducted to determine the optimum setting of the analog low-cut filter. We hoped to raise the filter as high as possible to reduce unwanted surface wave noise, but low enough to allow the deepest events of interest to be recorded. Tests using the geometry chosen during the walkaway tests showed that the optimum filter setting was 32 Hz. This value was lowered to 16 Hz along lines where reflections were difficult to see on field seismograph records.

Stacking tests were also conducted using the source–receiver geometry selected for the reflection lines. The source was fired repeatedly into the geophone spread in an attempt to increase the signal-to-noise ratio by partly cancelling random noise. Four source stacks per shotpoint were chosen as a reasonable compromise between improvement in data quality and the pace of the survey.

Other acquisition parameters chosen on the basis of these tests included a seismograph sampling interval of 1 ms, a record length of 1 s, and an anti-alias (high-cut) filter setting of 250 or 500 Hz (table 1).

Reflection Processing

Seismic reflection data acquired at Faskin Ranch were transferred each evening to a Macintosh computer and stored on 8-mm digital tape. After the field work was complete, the data were processed at UTEP on an IBM RS-6000 computer using the software ProMAX and at BEG on a Macintosh Quadra 700 computer using the software SPW. Processing procedures (table 2) were those common to many types of reflection processing (Yilmaz, 1987).

At BEG, the first processing step was to convert the data files from seismograph format to SPW format. Next, trace headers were created that combined the seismic data containing acquisition geometry information recorded by the seismograph operator and the surveyor. Dead or excessively noisy traces were deleted from the data set, which was then resampled to a 2-ms sample interval to reduce the size of the data set. A mute function was designed to delete the first arrivals from each shot gather to prevent them from stacking as a false reflector. Another mute function was designed to remove the air wave, or the sound of the source weight striking the ground plate, from each shot gather. Datum corrections were then made to each trace that effectively shifted them to a common elevation. Automatic gain control was applied to amplify weak arrivals at late times or far offsets. A dip filter was applied in the frequency–wavenumber domain to attenuate high-amplitude, slow-moving surface waves. This step was followed by shot deconvolution, which attempts to collapse the long and reverberatory source wavelet into a sharper wavelet that is easier to interpret on a stacked section. Velocity analysis was conducted by fitting reflection hyperbolas to events on common midpoint (CMP) gathers, or gathers of all traces that have the same source–receiver midpoint. In-24 fold data, there are 24 traces in a

Table 2. Processing steps, parameters, and purpose of each step used to convert seismic reflection data collected at Faskin Ranch to final seismic sections. Data processed using Seismic Processing Workshop (Parallel Geoscience) and ProMAX (Advance Geophysical).

Processing step	Parameters	Purpose
SEG-2 input	1 ms sample rate, 1 s record length	Convert seismic data from Bison format to processing format
Create trace headers	Seismic data, surveyor and observer notes	Combine acquisition geometry and shot records
Trace edit		Remove bad traces
Resample	2 ms sample rate	Reduce size of data set
Early and surgical mute		Mute first break and air wave
Datum correction	1324 m datum, 500 m/s velocity	Adjust all traces to common elevation datum
Automatic gain control	200 ms window	Amplify weak arrivals at late times or far offsets
Dip filter	Reject 25 to 500 m/s, <100 Hz	Attenuate surface waves
Shot deconvolution	Spiking, 0.1% whitening 100 ms inverse filter length 100 ms design window start 500 ms design window length	Shrink wavelet
Common midpoint sort		Collect all traces with same source–receiver midpoint (CMP)
Velocity analysis	Semblance plot, 400 to 2000 m/s Hyperbola picking	Pick stacking velocities for moveout correction
Bandpass filter	Pass 15 to 50 Hz, 18 dB/octave rolloff	Remove unwanted low- and high-frequency noise
Normal moveout correction	Velocity function every 20 to 50 CMP's	Simulate zero offset for all traces
Common midpoint stack	All traces	Stack all traces with same source–receiver midpoint (CMP)

CMP gather. A bandpass filter was then applied to remove unwanted low- and high-frequency noise.

The velocity function derived from the CMP gathers was used to correct each trace in the CMP gather for normal moveout (the delay in arrival time caused by increasing source–receiver offset) and to simulate zero offset in all traces. In the final processing step, each velocity-corrected trace in a CMP gather was summed to produce a single composite trace. A stacked seismic section is a display of these composite traces.

Surface Wave

The surface wave experiment was designed to examine the changes in shear velocity with depth. Phase information from surface waves can be used to determine physical properties of near-surface sediments. This experiment was conducted along reflection line LLRL1 at its intersection with line LLRL3 (fig. 4).

Two types of geophones were located at survey point 258 on line LLRL1 (table 1). A group of 12 8-Hz geophones were arranged in a 3.3-ft (1-m) square; ground motion detected by these geophones was summed into a single trace on the seismograph. In addition, ground motion was recorded at the same location by a single 40-Hz geophone. For each record, the geophones were left in the same position while the source was moved away from the geophones at 32.8-ft (10-m) increments. Distances between the source and receivers ranged from 32.8 to 1017.1 ft (10 to 310 m) and extended along line LLRL1 both to the northwest and to the southeast. One shot from the accelerated weight drop produced sufficient energy for the near offsets, but at farther offsets more shots per shotpoint were needed to produce adequate signal strength. A maximum of four shots per shotpoint was used at the farthest offsets. Data were recorded at 2-ms intervals for a total record length of 2 s. Analog low-cut filters were set to 4 Hz, the lowest possible setting. The high-cut filter was set to 250 Hz to prevent sample aliasing.

Borehole Velocity Survey

Downhole velocity data were acquired from borehole YM-63 (fig. 4) to determine a velocity profile of the shallow subsurface directly and allow calibration of the shallow reflection sections. Downhole data were acquired in May 1993 during the drilling of the borehole. A modified soil-probe hammer placed 9.8 ft (3 m) from the borehole was used as a seismic source, and a single hydrophone was used as the downhole receiver. The borehole was filled with drilling mud during the survey.

Seismic waves detected by the hydrophone were sampled by the seismograph at 1-ms intervals for 1 s after the source was fired. Shot records were acquired at 3.3-ft (1-m) increments between borehole depths of 6.6 and 193.6 ft (2 and 59 m). One shot yielded a sufficiently good signal-to-noise ratio to a depth of 167.3 ft (51 m); two or three shots were required when the hydrophone was between 170.6 and 193.6 ft (52 and 59 m) below the surface. First arrival times were picked for each depth using SPW and then were used to calculate average velocities to a given depth (equivalent to reflection stacking velocities) and interval velocities between depths.

RESULTS

Seismic Refraction

Five reversed and one unreversed seismic refraction spreads were acquired at Faskin Ranch (fig. 3) to determine seismic velocities of near-surface layers and to obtain rough estimates of basin-fill thickness. A sample field record (fig. 5) from refraction line LLRR1-4 includes surface waves, reflected waves, a direct arrival, and critically refracted arrivals. In refraction analysis, arrival times of the direct wave, which travels in the surface layer from the source to the receiver without being reflected or appreciably refracted, are used to determine the seismic velocity of layer 1. At source–receiver offset distances greater than about 115 ft

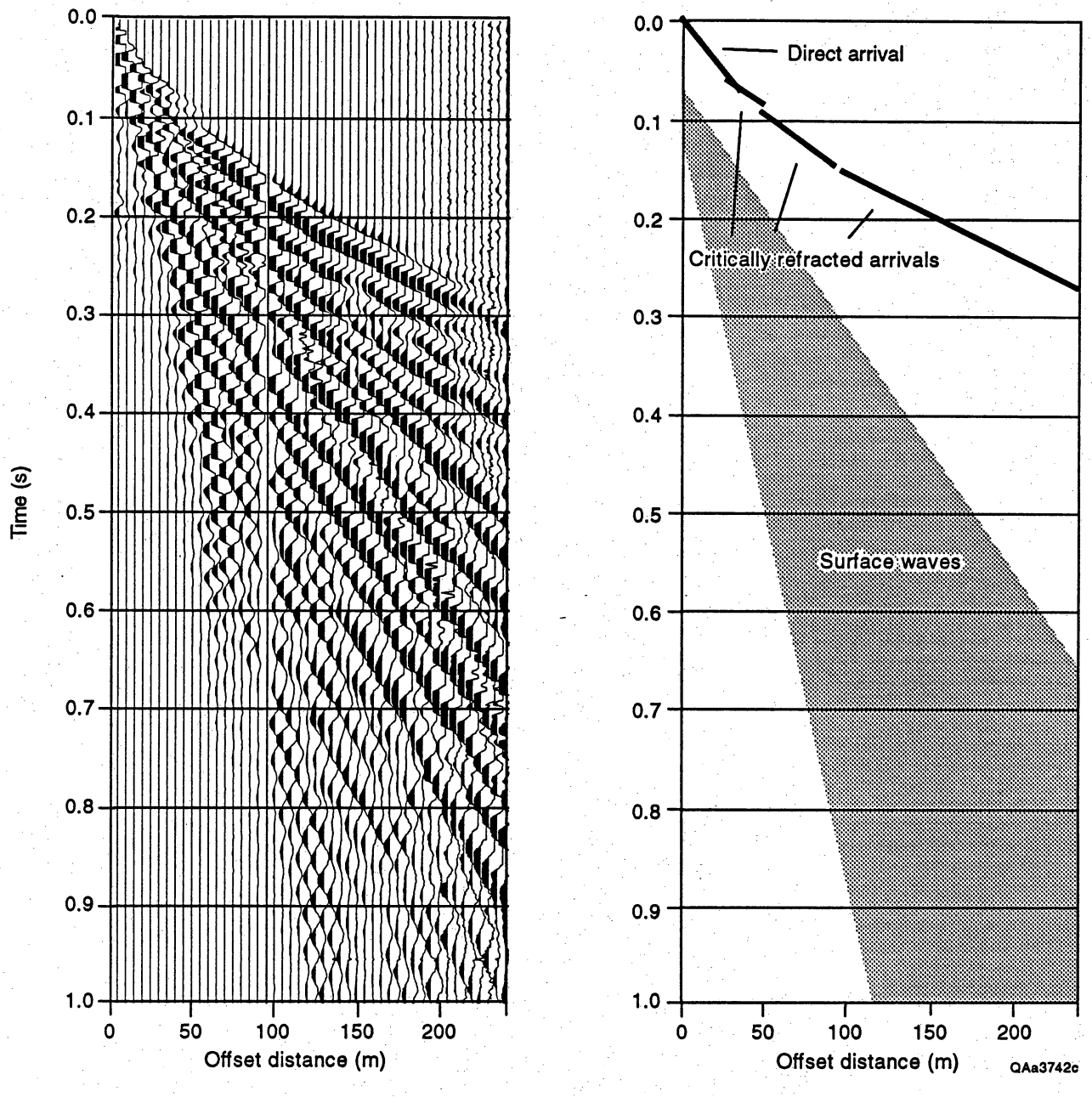

Figure 5. End-shot field record LLRR6005 (left) from refraction spread LLRR1-4 and interpreted record (right) showing direct arrival and refracted arrivals. Gain of 9 dB applied to field record to amplify weak arrivals.

(>~35 m) on the sample record, a critically refracted wave overtakes the direct wave and arrives first. Apparent velocities of layer 2 can be calculated from the offset distances and arrival times associated with the first refracted arrival. In addition, zero-offset intercept times of a line fitted to the first refractor arrival times can be used along with the velocities of the overlying layer to calculate the thickness of layer 1. At Faskin Ranch, a second critically refracted wave became the first arrival at offset distances larger than those shown on the sample field record. The second refracted arrival can be used to obtain layer 3 apparent velocities and layer 2 thicknesses in a manner similar to that of the first refracted arrival. Reversed refraction spreads can be used to determine the dip and true seismic velocities of detected layers.

Spread LLRR1-2

Refraction spread LLRL1-2 is oriented northwest-southeast (fig. 3) and is the westernmost refraction spread along reflection line LLRL1. First arrival times at shot to receiver distances of 8.2 to 1156.5 ft (2.5 to 352.5 m) indicate the presence of a direct wave and two critically refracted waves on both forward (shots to the northwest of the geophone spread) and reversed (shots to the southeast of the spread) sections (fig. 6). The direct wave was the first arrival between the source and an offset of 66 ft (20 m), where it was overtaken by the first refracted arrival to offsets of 902 ft (275 m) on forward data and 738 ft (225 m) on reversed data. The second critically refracted wave was the first arrival to the maximum offset of 1156 ft (352.5 m).

Linear least-squares fits to arrival time and offset distance pairs indicate apparent seismic velocities of 1224 and 1316 ft/s (373 and 401 m/s) for layer 1, 3337 and 3360 ft/s (1017 and 1024 m/s) for layer 2, and 6093 and 11122 ft/s (1857 and 3390 m/s) for layer 3 (fig. 6). True velocity and thicknesses can be calculated for layer 1 and true dip and velocity can be calculated for layer 2 from reversed data using the slope-intercept method (Palmer, 1986). These calculations suggest that layer 1 is 25.9 ft (7.9 m) thick and has a velocity of 1266 ft/s

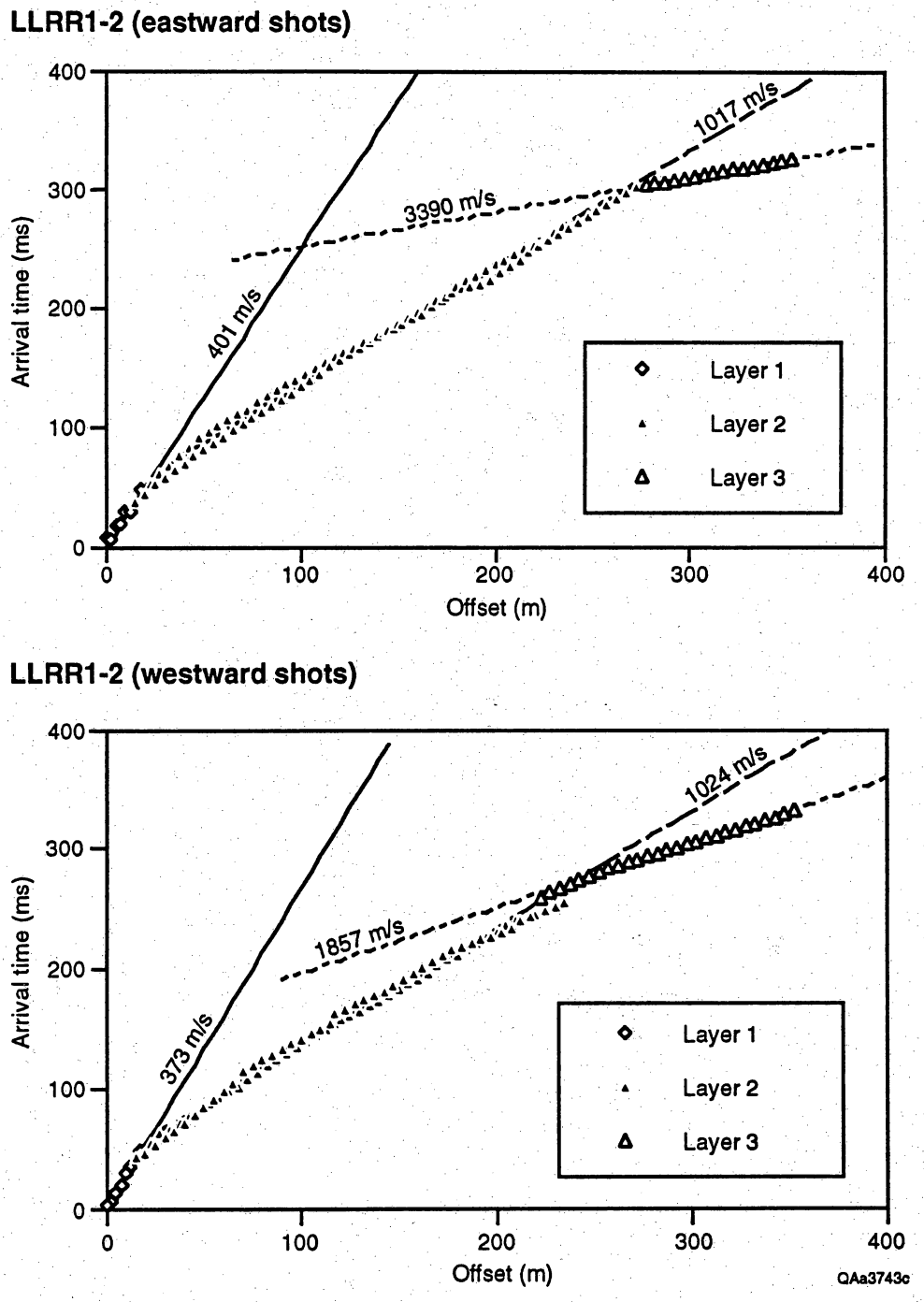

Figure 6. First-break times, layer assignments, and layer velocities of refraction spread LLRR1-2. Layer velocities in m/s.

(386 m/s) and layer 2 has less than a 1° dip and a velocity of 3350 ft/s (1021 m/s). The top of layer 2 is nearly horizontal. The large difference in velocities assigned to layer 3 suggests that the second critically refracted wave travels in different geologic horizons on the forward and reverse spread.

Layer 1, having low seismic velocities and relative thinness, probably represents loose and dry near-surface deposits. Layer 2 represents either the base of the soil zone or the upper limit of more competent basin-fill sediment. Its thickness and thus the depth to layer 3 must be used cautiously because it was calculated from best-fit lines through layer 3 time-distance pairs. Arrivals assigned to layer 3 occur over a small offset range (fig. 6), and lines fit to them have relatively large standard errors. Layer 3 probably represents different bedrock layers on the forward and reverse spreads. A bedrock depth estimate of 71 m (table 3) made from the reverse spread agrees most closely with a bedrock depth of 223 ft (68 m) at borehole YM-62, about 820 ft (250 m) northwest of the center of the spread.

Spread LLRR1-3

Refraction spread LLRR1-3, centered along reflection line LLRL1 771 ft (235 m) southeast of its intersection with reflection line LLRL3 (fig. 3), is an unreversed data set that includes only shots southeast of the geophone spread. First arrival times can be grouped into three sets relative to offset distance: the direct wave, which was the first arrival between the source and an offset of 66 ft (20 m); the first critically refracted wave, which was the first arrival between 66 and 820 ft (20 and 250 m); and the second critically refracted wave, which was the first arrival between 820 and 1157 ft (250 and 352.5 m) (fig. 7). The uncorrected three-layer velocity model that fits these arrival times includes a 32-ft (9.8-m) thick surface layer having a velocity of 1427 ft/s (435 m/s), a 298-ft (90.9-m) thick second layer having an apparent velocity of 3150 ft/s (960 m/s), and a third layer having an apparent velocity of 12867 ft/s (3922 m/s) (table 3).

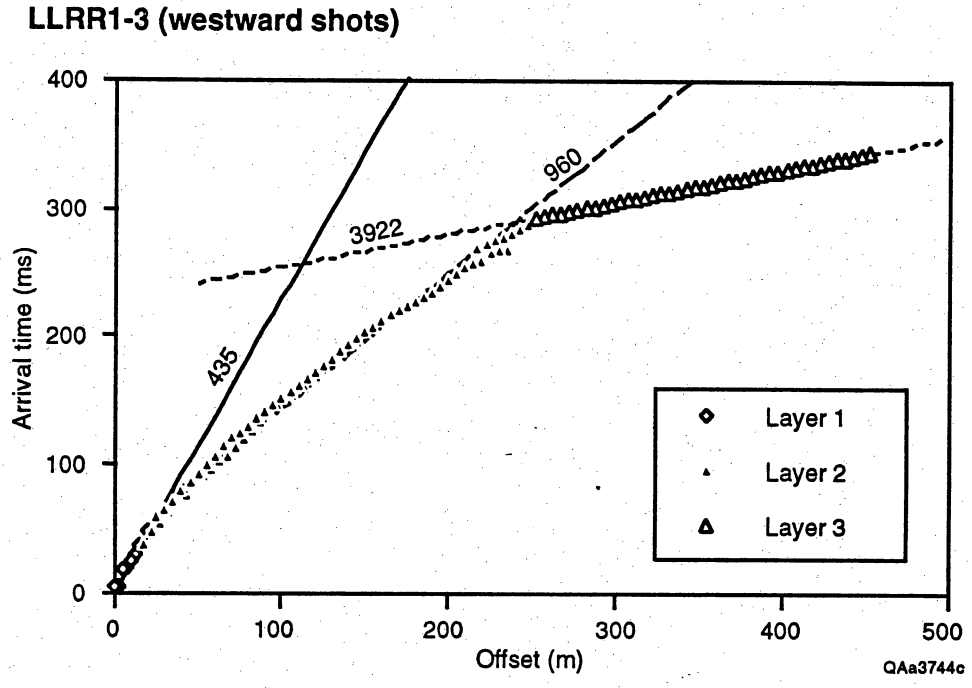

Figure 7. First-break times, layer assignments, and layer velocities of unreversed refraction spread LLRR1-3. Layer velocities in m/s.

Table 3. Summary of reversed refraction data from Faskin Ranch. Velocities, thicknesses, and dips calculated using slope-intercept method (Palmer, 1986). Positive dips to the southeast for NW–SE spreads and to the northeast for SW–NE spreads.

Refraction spread	Layer	Velocity (m/s)	Dip (°)	Layer thickness (m)	Depth to top (m)	Elevation at top (m)	Two-way time at top of layer (s)
LLRR1-2	1	386.4	0.0	7.9	0.0	1330	0.000
(NW–SE)	2	1020.6	0.1	63.0	7.9	1322	0.041
	3*	1857.1	–	–	70.9	1259	0.164
LLRR1-3**	1	435.3	0.2	9.8	0.0	1331	0.000
(NW–SE)	2	959.7	–	90.9	9.8	1321	0.045
	3	3921.8	–	–	100.7	1220	0.237
LLRR1-4	1	379.3	0.2	8.9	0.0	1328	0.000
(NW–SE)	2	947.6	1.6	57.7	8.9	1319	0.047
	3	2502.5	8.0	–	66.6	1261	0.169
LLRR2	1	421.7	–0.2	7.2	0.0	1330	0.000
(SW–NE)	2	1031.9	–0.6	96.7	7.2	1323	0.034
	3	3785.0	–2.5	–	103.8	1226	0.221
LLRR3	1	441.0	–0.2	10.1	0.0	1332	0.000
(SW–NE)	2	987.3	–1.0	106.6	10.1	1322	0.046
	3	8106.5	–2.7	–	116.7	1215	0.262
LLRR4	1	397.1	0.0	17.7	0.0	1328	0.000
(SW–NE)	2	1106.4	–1.6	82.0	17.7	1310	0.089
	3	4850.9	–7.3	–	99.7	1228	0.237

*Layer 3 arrival may not be the same geologic unit on forward and reverse spreads; layer 3 velocity and layer 2 thickness are from reverse data only.
** Spread unreversed

Because the spread is unreversed, velocities of layers 2 and 3 and thicknesses of layers 1 and 2 cannot be corrected to account for dipping layers. The depth estimate of the top of layer 2, 32 ft (9.8 m), is probably a good estimate because the layer-2 velocity is reasonably close to that of other refraction spreads. Estimated depth to layer 3 (328 ft [100 m]), however, is less reliable because the top of layer 3 is probably a dipping interface. The refractor associated with layer 3 probably represents a bedrock refractor. The nearest borehole is YM-4, about 1640 ft (500 m) northwest of the center of the refraction spread (fig. 3). Bedrock depth at this borehole is greater than 250 ft (>76 m) (fig. 2).

Spread LLRR1-4

Reversed refraction spread LLRR1-4, located along reflection line LLRL1, is centered at its intersection with reflection line LLRL4 (fig. 3). First arrivals (fig. 8) were (1) the direct wave between the source and an offset of 49 ft (15 m), (2) the first critically refracted wave 49 to 623 ft (15 and 190 m) from shots west of the geophone spread to 820 ft (250 m) from shots east of the geophone spread, and (3) a second critically refracted wave to the maximum offset of 1157 ft (352.5 m).

Corrected velocities and thicknesses of the three-layer model (table 3) include a surface layer 29 ft (8.9 m) thick having a velocity of 1243 ft/s (379 m/s), an underlying layer 189 ft (57.7 m) thick having a velocity of 3110 ft/s (948 m/s), and a basal layer having a velocity of 8212 ft/s (2503 m/s).

The calculated depth to the top of layer 3 is 220 ft (67 m), which is almost 131 ft (40 m) less than the depth to layer 3 calculated for crossing refraction spread LLRR4 (fig. 3 and table 3). Velocities at the top of layer 3 are also greatly lower for refraction spread LLRR1-4, suggesting that layer 3 does not represent bedrock at LLRR1-4 but rather a competent horizon within the basin fill. Nearest known depths to bedrock are 164 ft (50 m) at borehole YM-5, 2300 ft (700 m) south of the center of the spread, and 679 ft (207 m) at borehole YM-63, 1640 ft (500 m) north of the center of the spread (fig. 2). Layer 3 at refraction spread LLRR1-4 may represent a primary lithologic change or a secondary lithologic change such as a zone of pedogenic carbonate accumulation.

Spread LLRR2

A reversed refraction data set was collected at site LLRR2, along reflection line LLRR2 and centered at the intersection with reflection line LLRR1 (fig. 3). First arrivals fell on three lines on both forward and reverse data sets (fig. 9), representing a direct wave and two critically refracted waves. The direct wave was the first arrival on both data sets to an offset of 49 ft

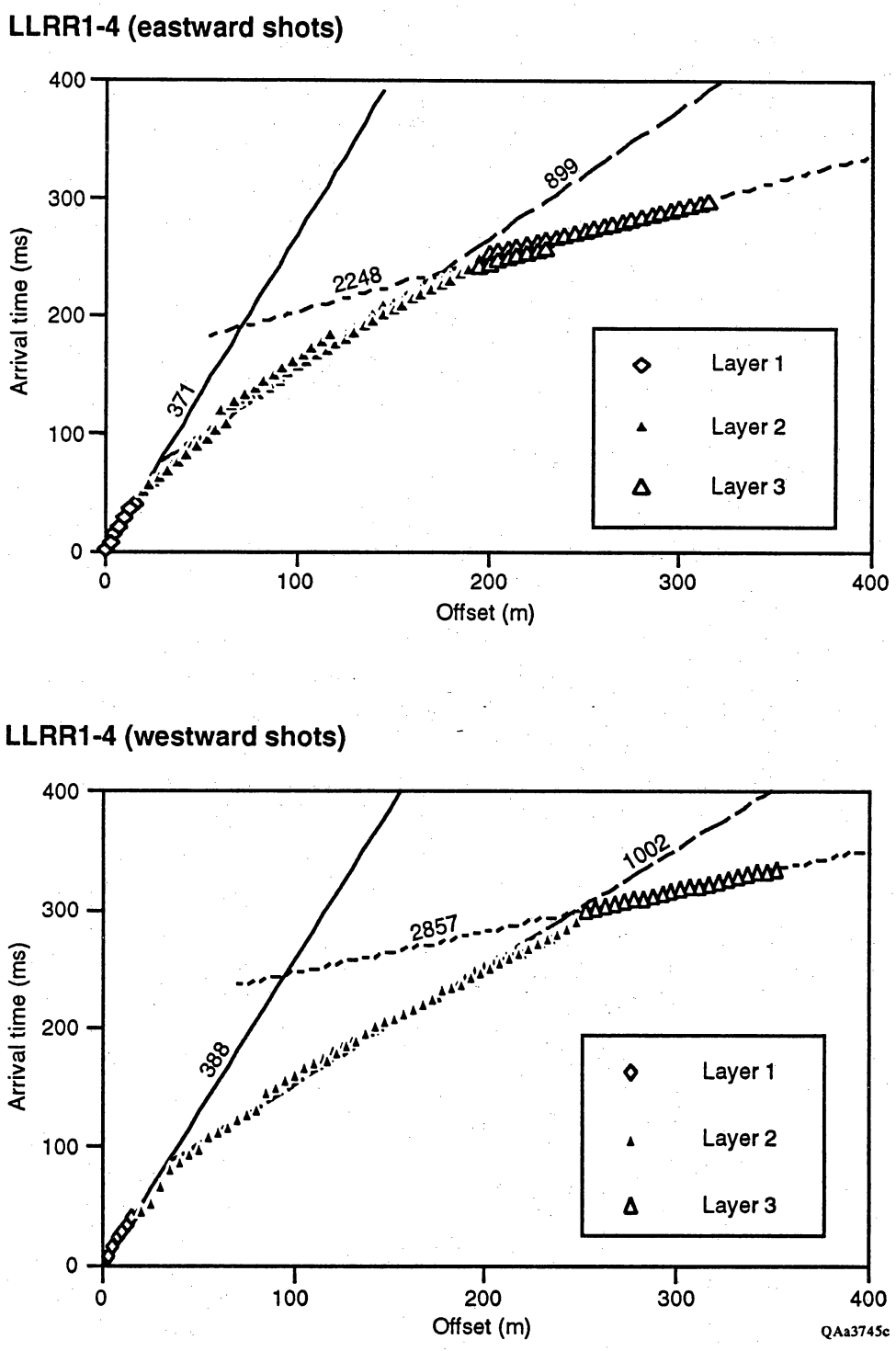

Figure 8. First-break times, layer assignments, and layer velocities of refraction spread LLRR1-4. Layer velocities in m/s.

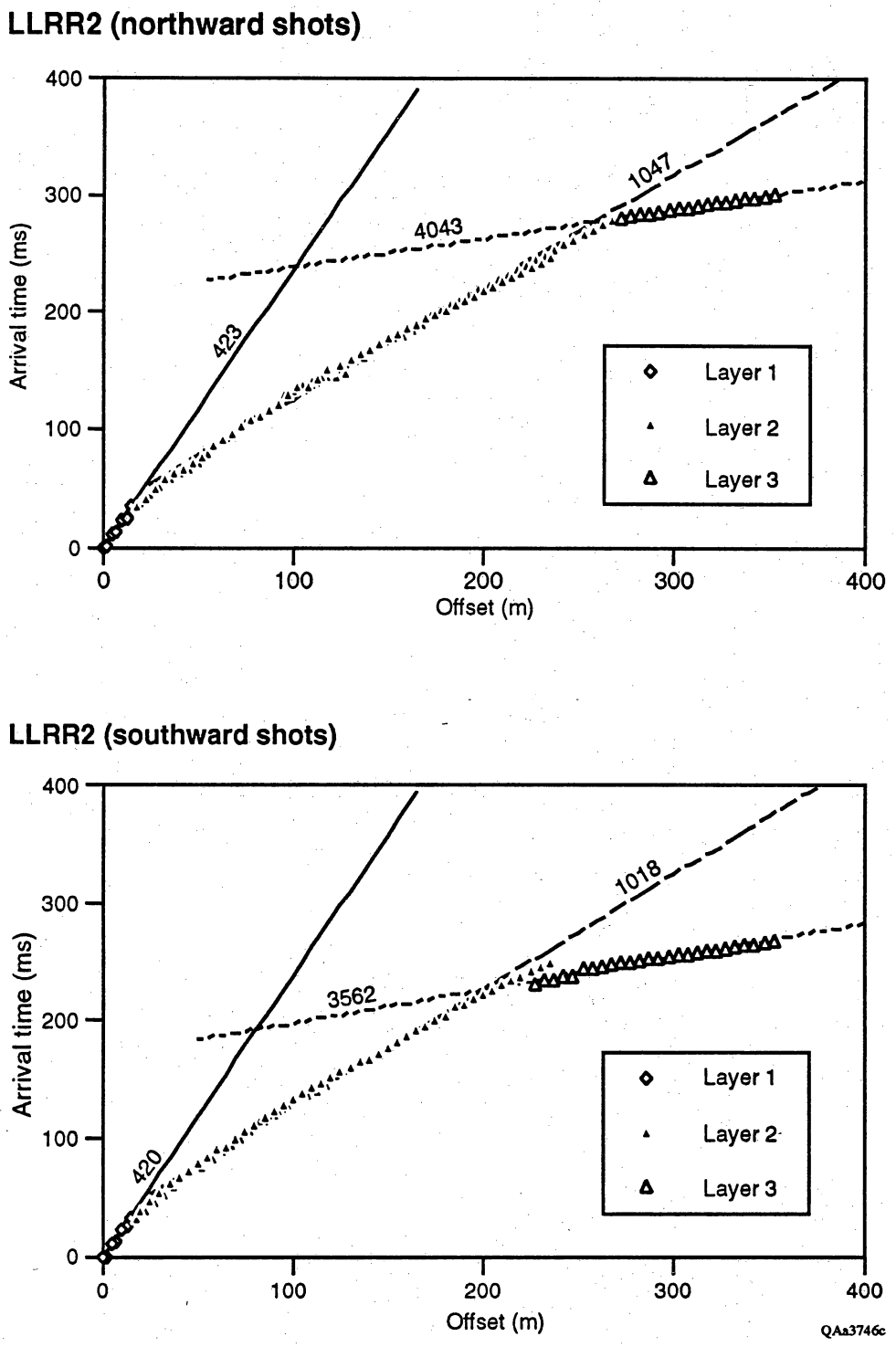

Figure 9. First-break times, layer assignments, and layer velocities of refraction spread LLRR2. Layer velocities in m/s.

(15 m), where it was overtaken by the first critically refracted wave to an offset of 886 ft (270 m) with shots southwest of the recording spread and to an offset of 755 ft (230 m) with shots northeast of the spread. A second critically refracted wave was the first arrival to the maximum offset recorded.

A corrected three-layer model of these data (table 3) consists of a surface layer 24 ft (7.2 m) thick having a velocity of 1385 ft/s (422 m/s), an intermediate layer 318 ft (97 m) thick having a velocity of 3386 ft/s (1032 m/s), and a basal layer having a velocity of 12418 ft/s (3785 m/s). Lines fitted to layer 3 refracted arrivals are relatively uncertain because of the limited offset range for which they were the first arrival, particularly for the shots located south of the geophone spread. As a result, the thickness calculated for layer 2 and depth to the top of layer 3 are gross estimates that differ from the bedrock depth of 223 ft (68 m) found at nearby borehole YM-62 (fig. 2). Layer 3 probably does represent a layer within bedrock, but the top of layer 3 may not coincide with the top of bedrock if the bedrock surface is highly fractured, deeply weathered, or underlain by bedrock material having velocities high enough to cause an overlying bedrock layer that has slower seismic velocities to be hidden.

Spread LLRR3

Reversed refraction spread LLRR3 is centered along reflection line LLRL3 about 787 ft (240 m) north of the intersection with reflection line LLRL1 (fig. 3). A direct wave was the first arrival (fig. 10) between the source location and an offset of 66 ft (20 m), the first critically refracted wave was the first arrival from 66 ft (20 m) to an offset of between 820 and 984 ft (250 and 300 m), and a second critically refracted wave was the first arrival in the relatively short offset range between 919 and 1157 ft (280 and 352.5 m). Between the major arrivals were short segments that may represent intermediate layers, particulary between the first and second critically refracted arrivals after the northward shots and between the direct and first critically refracted arrivals after the southward shots. These intermediate layers were difficult to

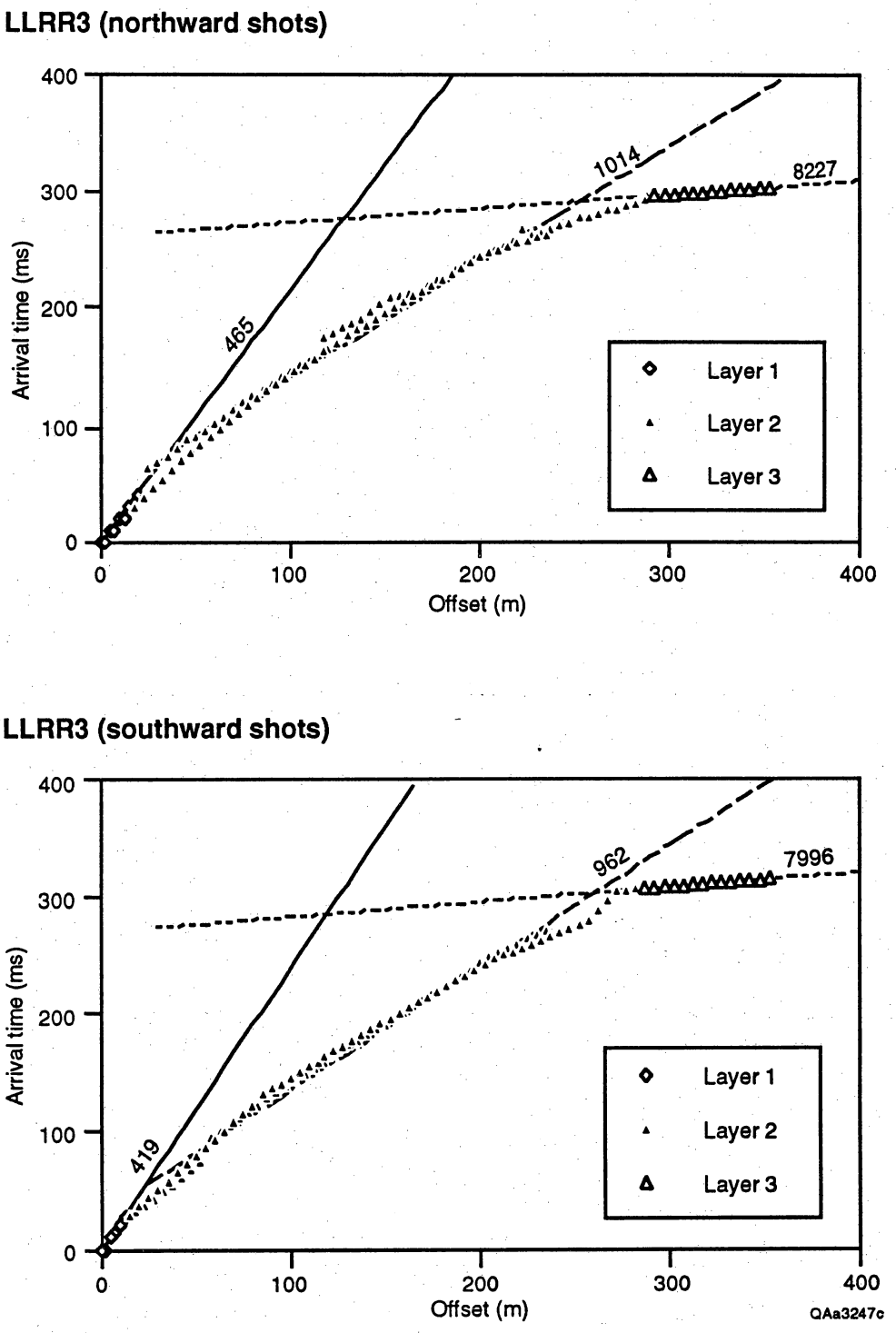

Figure 10. First-break times, layer assignments, and layer velocities of refraction spread LLRR3. Layer velocities in m/s.

quantify and were excluded from the model calculations, which reduces the accuracy of layer 2 and layer 3 depth calculations made from the reversed data.

Calculations of depth and velocity made from reversed data indicate that layer 1 is 33 ft (10 m) thick and has a velocity of 1447 ft/s (441 m/s), layer 2 is 351 ft (107 m) thick and has a velocity of 3238 ft/s (987 m/s), and layer 3 has a calculated velocity of 26595 ft/s (8106 m/s). The velocity of layer 3 is too high for the bedrock lithologies present near Faskin Ranch. These high velocities again probably result from calculations made from a limited range of first arrivals for the second critically refracted wave. These measurement difficulties also reduce the accuracy of layer-2 thickness and, consequently, the depth-to-bedrock calculation. Depth to bedrock at this site is estimated to be greater than 384 ft (>117 m). Borehole YM-4, only about 500 ft (150 m) from the center of the spread, did not reach bedrock at a total depth of 250 ft (76 m).

Spread LLRR4

Reversed refraction spread LLRR4 lies along reflection line LLRL4 and is centered at its intersection with reflection line LLRR1 (fig. 3). The direct wave was the first arrival along this spread to source–receiver offsets of 98 ft (30 m) (fig. 11). The first critically refracted wave was the first arrival at offsets between 98 and 850 ft (30 and 260 m), and a second critically refracted wave was the first arrival to the maximum offset recorded. Corrected velocities are 1303 ft/s (397 m/s) for layer 1, 3629 ft/s (1106 m/s) for layer 2, and 15915 ft/s (4851 m/s) for layer 3 (table 3). Corrected thicknesses are 58 ft (17.7 m) for layer 1 and 269 ft (82 m) for layer 2.

Layer-3 velocities are poorly constrained because the offset range of the second refracted arrival is limited. Consequently, the thickness of layer 2 (269 ft [82 m]) and the depth to the top of layer 3 (328 ft [100 m]) are rough estimates. Layers 1 and 2 have velocities that are similar to those of crossing refraction spread LLRR1-4, but the layer-3 velocity is higher and the

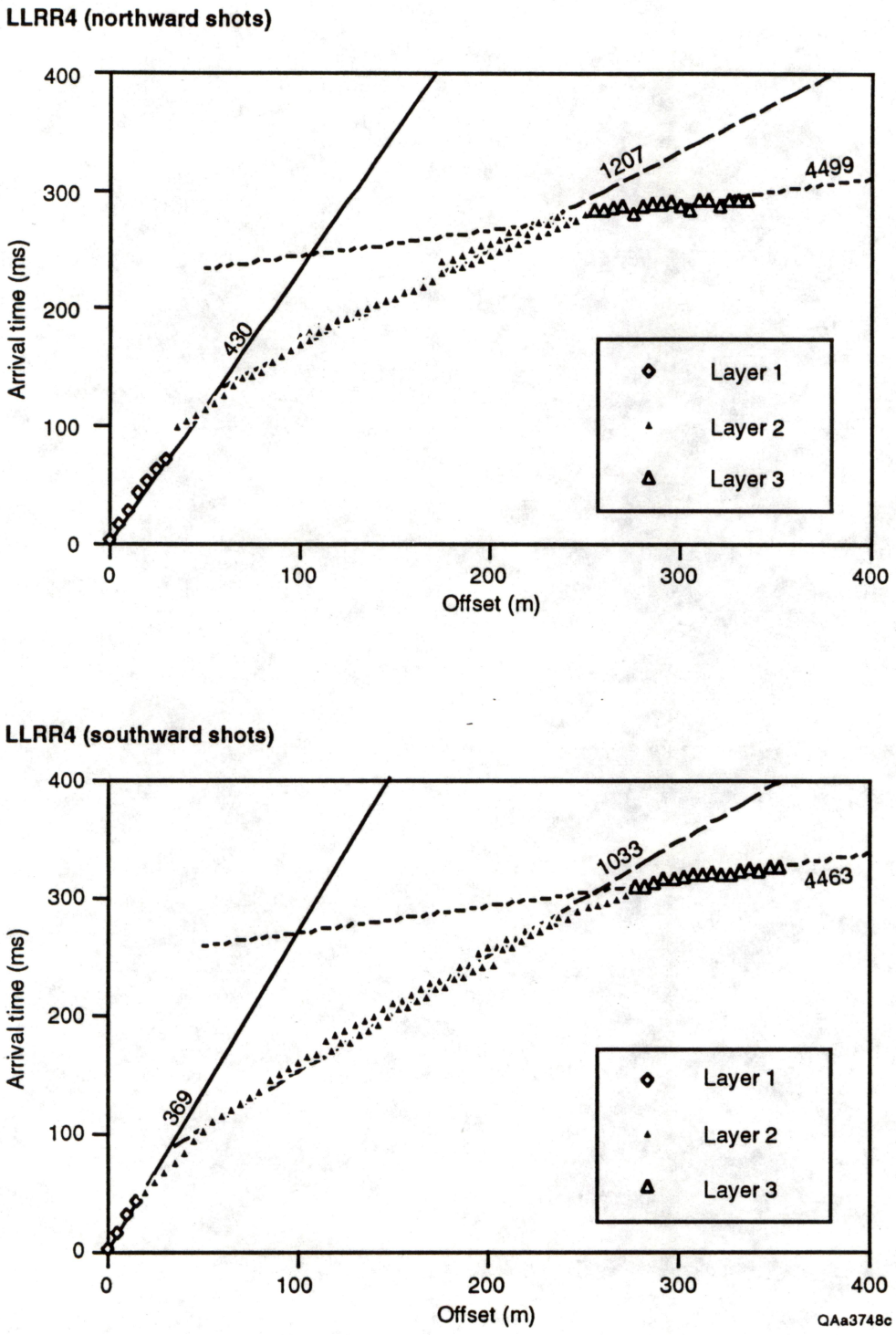

Figure 11. First-break times, layer assignments, and layer velocities of refraction spread LLRR4. Layer velocities in m/s.

depth estimate to the top of layer-3 is deeper at spread LLRR4. These observations confirm that layer 3 at LLRR1-4 is not the top of bedrock.

Seismic Reflection

Nearly 3.9 mi (6.2 km) of shallow seismic reflection data were collected along four lines across Faskin Ranch (fig. 4) to determine basin geometry (depth to bedrock) and internal stratigraphy of the basin fill. Data quality (assessed in terms of how evident reflectors are on field records, processed trace gathers, and stacked final sections) ranges from good to poor (fig. 12). Two factors contributed to the difficulty in obtaining uniformly good data across the site: first, seismic waves are rapidly attenuated in areas such as Faskin Ranch, where the water table is deep, surface sediments are loose (most of the proposed site is mantled by windblown sand), and the basin fill is poorly consolidated; second, the acquisition geometry of lines LLRL2, LLRL3, and LLRL4 was optimized for expected bedrock depths of 164 to 300 ft (50 to 91 m) as indicated by existing boreholes and gravity data. Refraction data, further drilling, and initial analysis of reflection data revealed considerably deeper bedrock on the north half of the site. Consequently, acquisition geometry was lengthened for the last line collected (LLRL1, table 1) and the bedrock image improved.

Data quality varied even along a single reflection line having the same acquisition geometry because of varied surface and subsurface characteristics, nearby power lines, and wind noise. Data were good along most of line LLRL1, except for a short segment of poor data between CMP 125 and 175 (fig. 12). Data were fair to good along the southern two-thirds of line LLRL2 and were poor at the north end. Data were good at the south half of line LLRL3 and worsened along the north half where the basin deepens. Fair data were collected at the north and south ends of line LLRL4; data quality was poor in the center of this line. Confidence in interpretations of the bedrock reflectors along these lines is higher where data quality is good or where nearby boreholes reach bedrock.

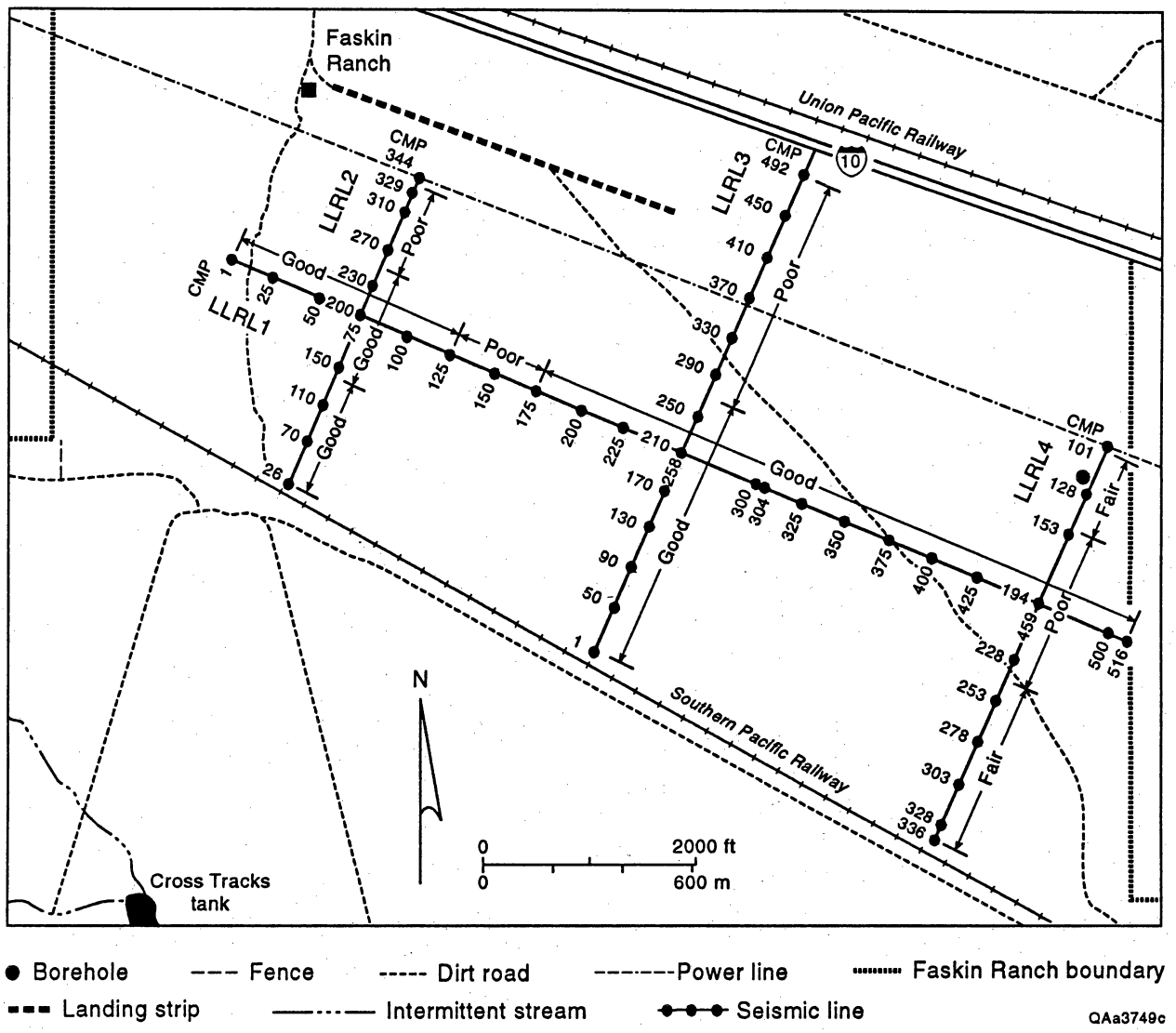

Figure 12. Qualitative assesment of data quality along seismic reflection lines LLRL1, LLRL2, LLRL3, and LLRL4.

Time-to-Depth Conversion

Seismic sections are presented in the time domain and must be converted to the distance domain to estimate depths of reflectors. A velocity function, or the relationship between seismic velocity and depth or time, is used to make this time to depth conversion. Velocity information at Faskin Ranch was derived from three sources: refraction surveys, reflection data, and a borehole velocity survey.

Velocity models constructed from refraction surveys indicated the presence of a thin, low-velocity layer near the surface (1243 to 1447 ft/s [379 to 441 m/s], table 3) that overlies a thicker, higher velocity layer (3110 to 3629 ft/s [948 to 1106 m/s]) that represents most of the basin fill. These models yield velocity profiles that are adequate for time corrections to bring all reflection traces to a common elevation. They were also used during the initial stages of velocity analysis to obtain preliminary stacks of the reflection data.

Velocity information is also contained within the reflection data. Gathers of traces having a common midpoint and multiple source–receiver distances ideally contain reflectors that cross the gather in a hyperbolic curvature. A hyperbola fitted to a given reflector has a unique velocity and zero offset associated with it; the curvature of these hyperbolas decreases with increasing seismic velocities. Time and velocity pairs were picked for common midpoint gathers at regular intervals along each of the seismic lines (fig. 13). These velocity picks fall in a relatively narrow range, particularly earlier than 0.3 s two-way time, and show a general increase with time. Best-fit lines calculated for each of the seismic lines are similar (table 4) and result in similar velocities of given two-way times in the time range of interest. A composite velocity function (fig. 13 and table 4) was obtained by least-squares analysis of velocity picks from lines LLRL1, LLRL2, and LLRL3 along which data quality was higher than along LLRL4. This function was used to convert time picks on each of the lines to estimated depths.

Combined field records from a borehole velocity survey at well YM-63 (figs. 12 and 14) show that the first arrival was increasingly delayed as the seismic receiver was lowered in the

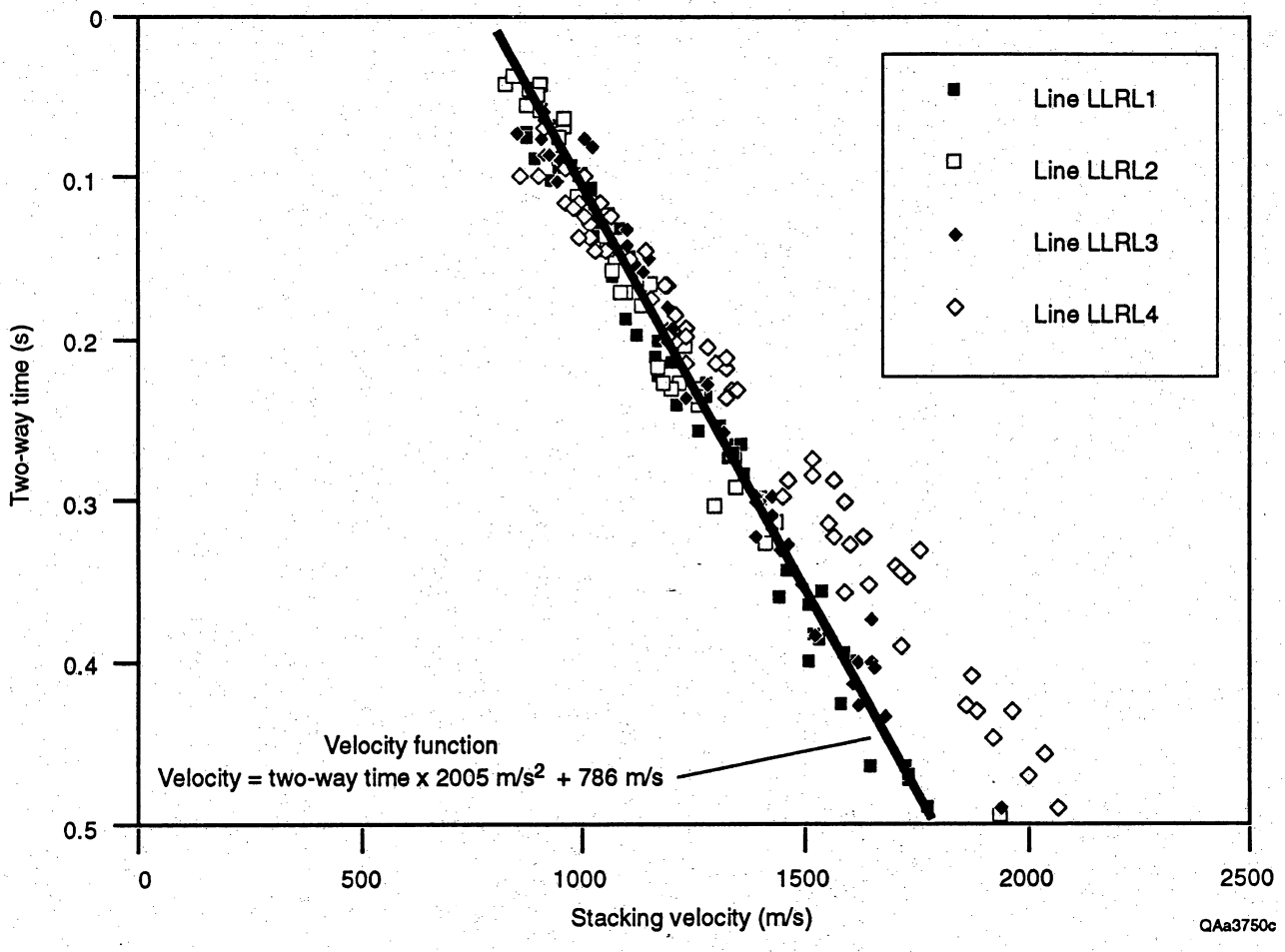

Figure 13. Stacking velocities picked from CMP gathers for reflection lines LLRL1, LLRL2, LLRL3, and LLRL4 and best-fit velocity function calculated from all lines except LLRL4.

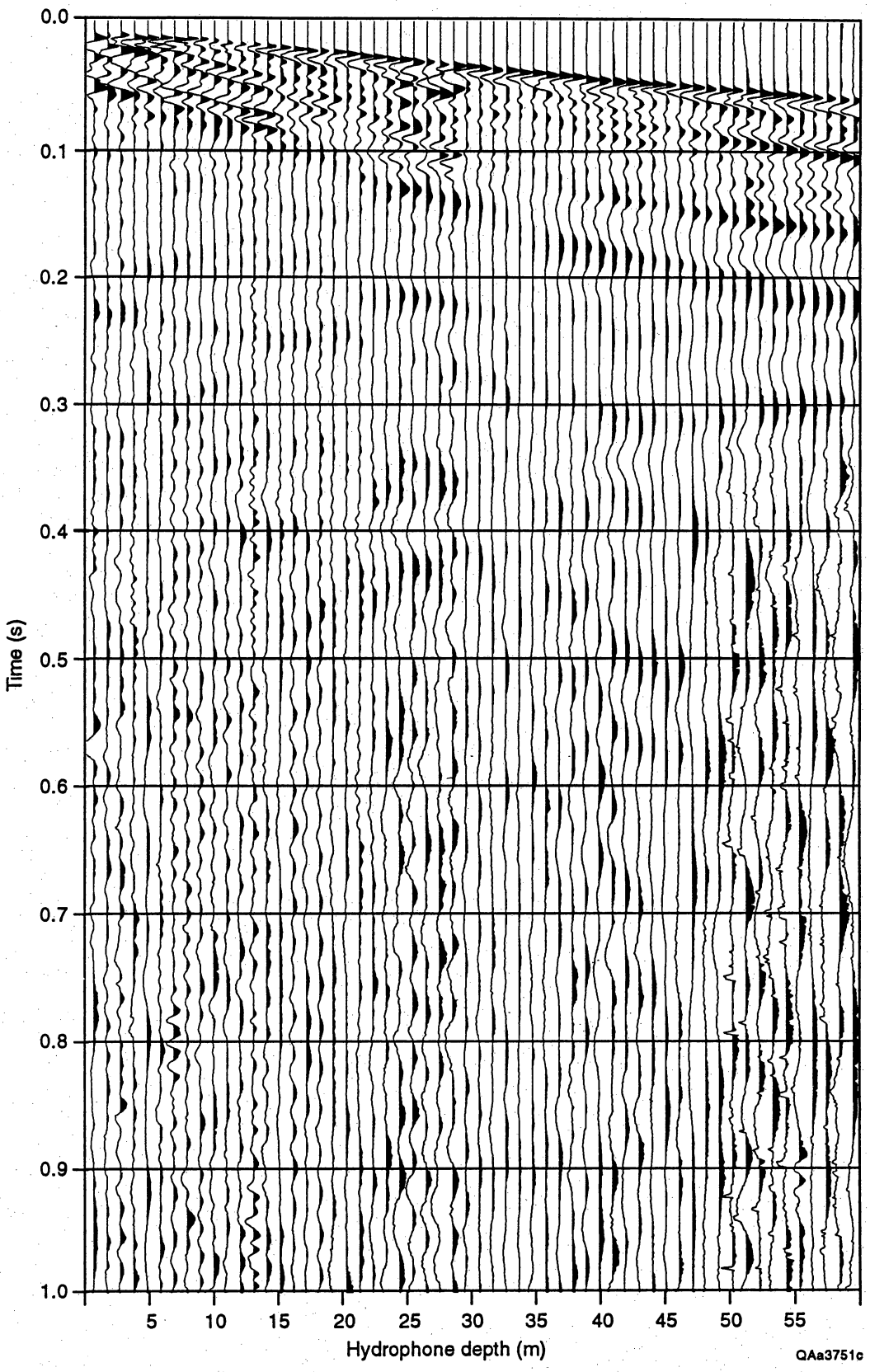

Figure 14. Combined field record from velocity survey at well YM-63. Seismic source was at the surface 3 m from borehole. Hydrophone was lowered into mud-filled borehole at 3-ft (1-m) increments from depth of 7 to 190 ft (2 to 59 m). First arrivals for each trace were used to calculate a seismic velocity profile. Display is a relative amplitude plot having automatic gain control over a 250-ms window.

borehole. Average velocities to a given depth were calculated by dividing the distance between the source and receiver by the time elapsed between the firing of the source and the first arrival at the receiver. These calculations indicate that the velocities increase rapidly in the shallow subsurface (fig. 15), from less than 1640 ft/s (<500 m/s) at receiver depths of 6.6 to 9.8 ft (2 to 3 m) to about 2625 ft/s (~800 m/s) at a receiver depth of 32.8 ft (10 m). Velocities continue to rise to the deepest level investigated (3280 ft/s [1000 m/s] at a receiver depth of 194 ft [59 m]), but at a lower rate. These velocities agree with the upper two layers of the refraction models and with the shallower velocity picks from the reflection data. A velocity function (fig. 15) was calculated from the borehole data for deeper than the deepest receiver level by extrapolating a best-fit line constructed from velocities to receiver levels deeper than 82 ft (25 m). This function was used to stack initial seismic sections and to guide velocity picks on actual reflection records.

Table 4. Velocity functions calculated from stacking velocity picks on reflection lines LLRL1, LLRL2, LLRL3, and LLRL4.

Line	Number of picks	Slope (m/s^2)	Intercept (m/s)	Slope (m/s^2)	Intercept (m/s)	r^2
LLRL1	81	1882.7	792.3	25.4	9.5	0.986
LLRL2	51	2088.7	773.0	40.6	12.3	0.982
LLRL3	76	2155.2	771.8	30.7	10.6	0.985
LLRL4	79	2867.3	670.9	37.3	11.5	0.987
Composite (1,2,3)	208	2005.5	786.5	21.9	7.6	0.976

Line LLRL1

Line LLRL1, 1.6 mi (2.6 km) long, ties to line LLRL2 at CMP 78, to line LLRL3 at CMP 258, and to line LLRL4 at CMP 459 (fig. 12). Data quality improves along this line than along other lines, several reflectors becoming visible within both basin fill and bedrock (fig. 16). The strongest reflector on the line is thought to be the bedrock reflection, which arrives progressively later to the southeast. Arrival times at the northwest end of the line are between

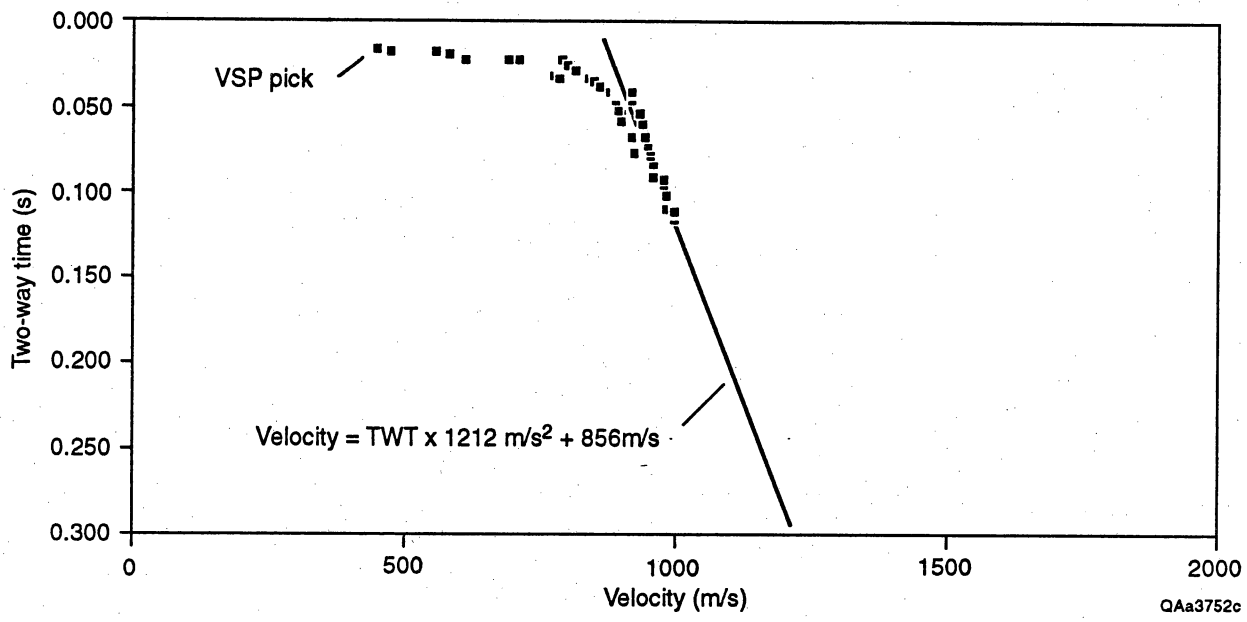

Figure 15. Velocity profile to 0.120 s derived from velocity survey of well YM-63. Velocity function calculated from velocity survey arrival times below 25-m hydrophone depth.

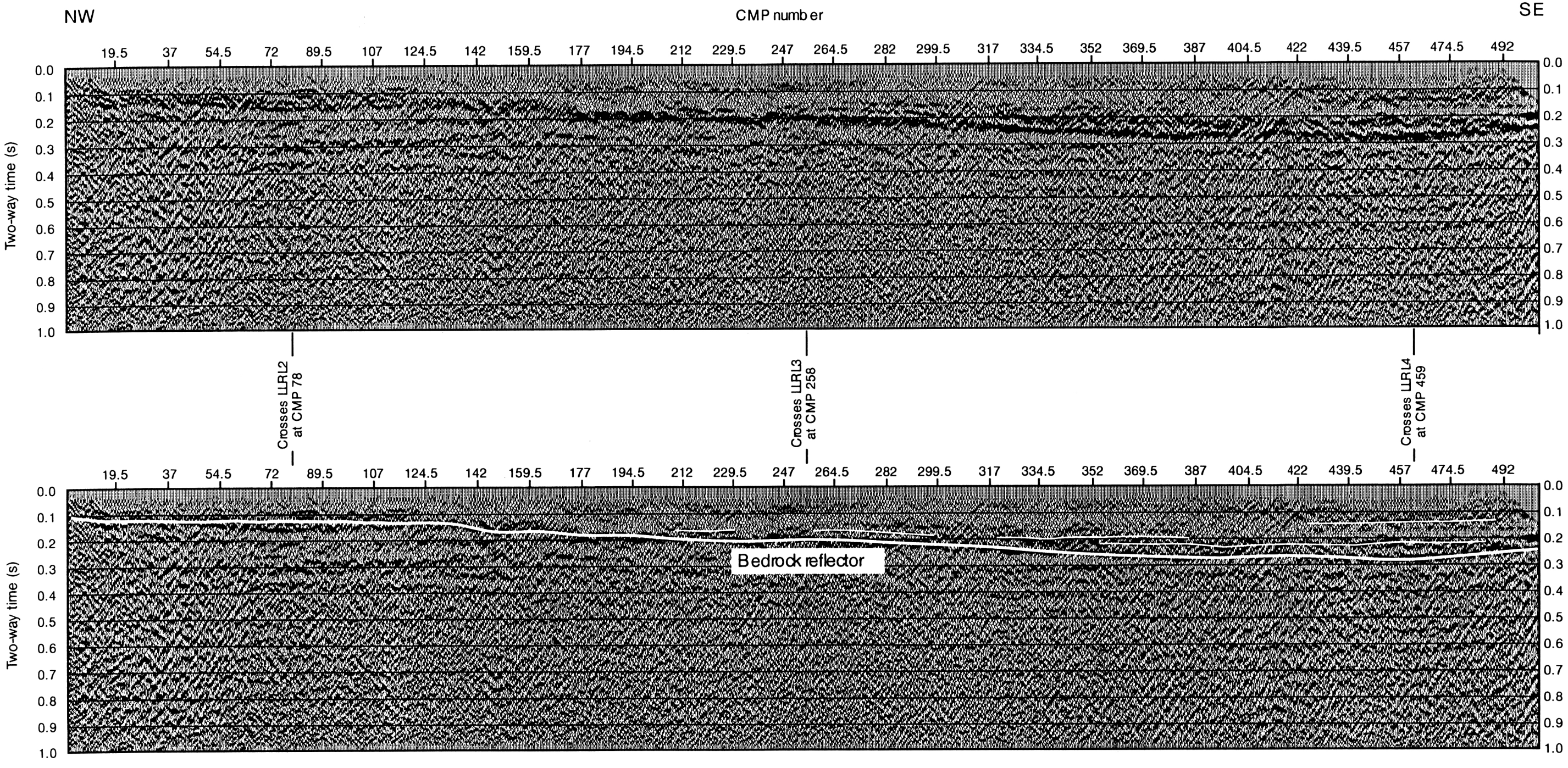

Figure 16. Faskin Ranch seismic reflection line LLRL1. Uninterpreted section at top; interpreted section at bottom. Heavy line represents interpreted bedrock reflector and lighter lines represent interpreted reflectors within the basin fill. Trace spacing 2.5 m. True amplitude display having automatic gain control applied. CMP locations shown in fig. 12.

100 and 150 ms, whereas arrival times at the southeast end are 250 to 300 ms. This reflector is difficult to follow between CMP's 142 and 177 perhaps because the bedrock surface dips too steeply.

Internal basin-fill reflectors are thought to be present at the southeast half of the line where the basin is relatively deep. Two-way times for these reflectors are 150 ms or later. Several of these reflectors appear to onlap to the northwest onto the bedrock surface. Relatively little reflected energy is returned to the surface above 100 ms. Bedrock reflectors are present to about 400 ms at the northwest end of the line and to perhaps 600 ms at the southeast end of the line. Many of these reflectors have gentle apparent dips to the northwest.

Two-way times picked for the interpreted bedrock reflector were converted to depths using the composite velocity function calculated from velocity picks (fig. 14). Elevations at the top of bedrock decrease from near 4183 ft (1275 m) at the northwest end of the line to 3773 ft (1150 m) near the southeast end of the line (fig. 17) and then begin to rise near the southeast end of the line. Because little relief exists at the surface, changes in estimated basin-fill thickness (fig. 18) mirror changes in bedrock elevation. Basin-fill thickness increases from about 197 to almost 650 ft (60 to 200 m) from northwest to southeast.

Line LLRL2

Reflection line LLRL2, 3110 ft (948 m) long, crosses line LLRL1 at CMP 200 (fig. 12). A bedrock reflection (fig. 19) is not as clear on this line as it is on LLRL1, but a correlative reflector does occur between 100 and 150 ms near the intersection of the two lines that can be followed most of the way across the section. This reflector deepens to the northeast, from 100 to 120 ms two-way time at the south third of the line to nearly 200 ms at CMP 274 where the interpreted bedrock reflector fades. A fairly clear reflector is present within the interpreted basin fill at about 90 to 100 ms between CMP's 99 and 291. Several reflector

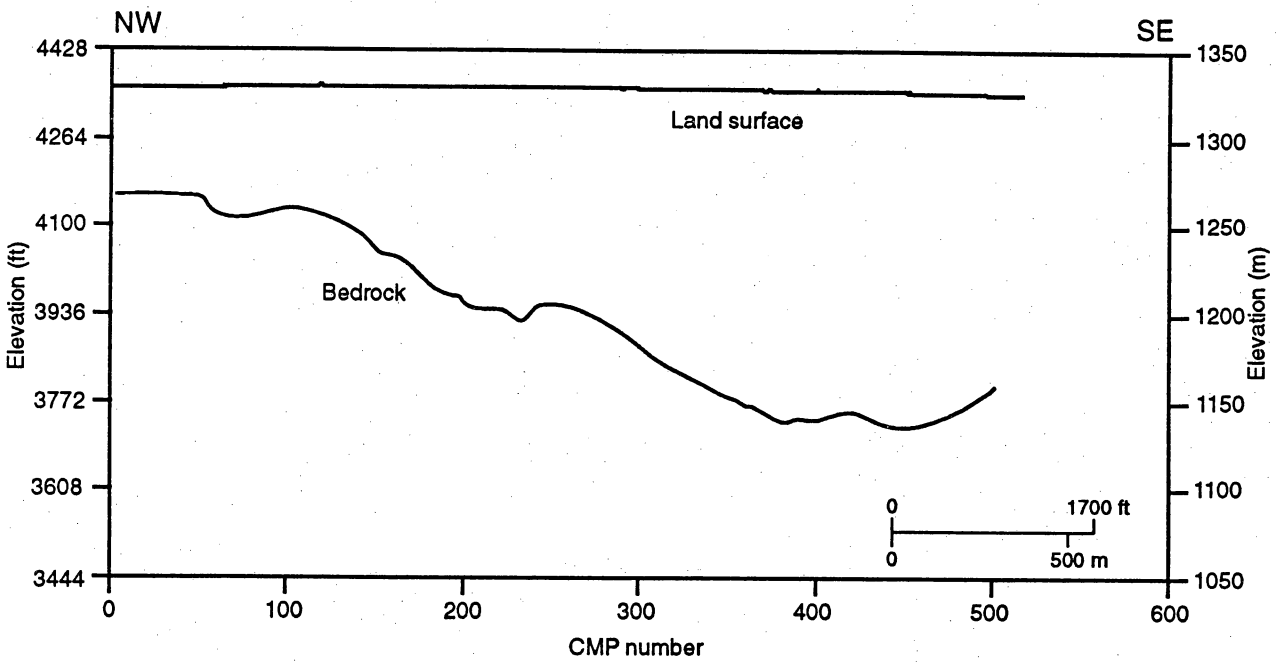

Figure 17. Land surface and estimated bedrock elevations for reflection line LLRL1. CMP locations shown in fig. 12. Vertical exaggeration = 5×.

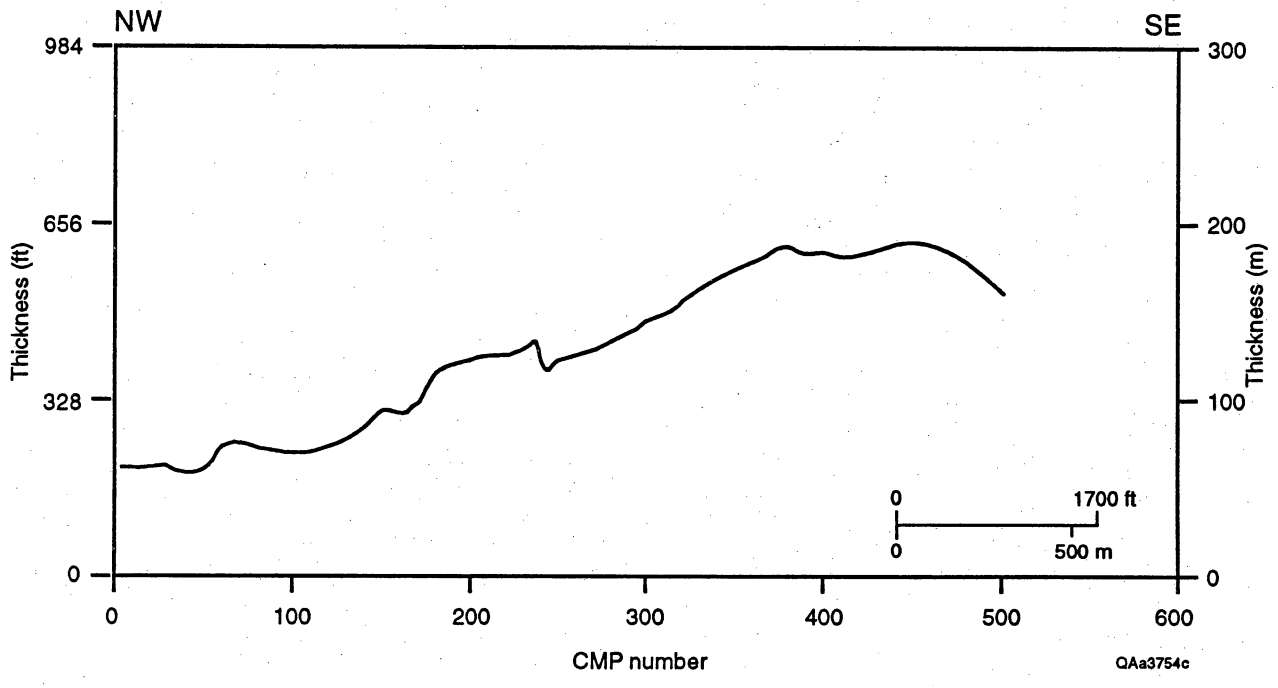

Figure 18. Estimated basin-fill thickness beneath reflection line LLRL1. CMP locations shown in fig. 12. Vertical exaggeration = 5×.

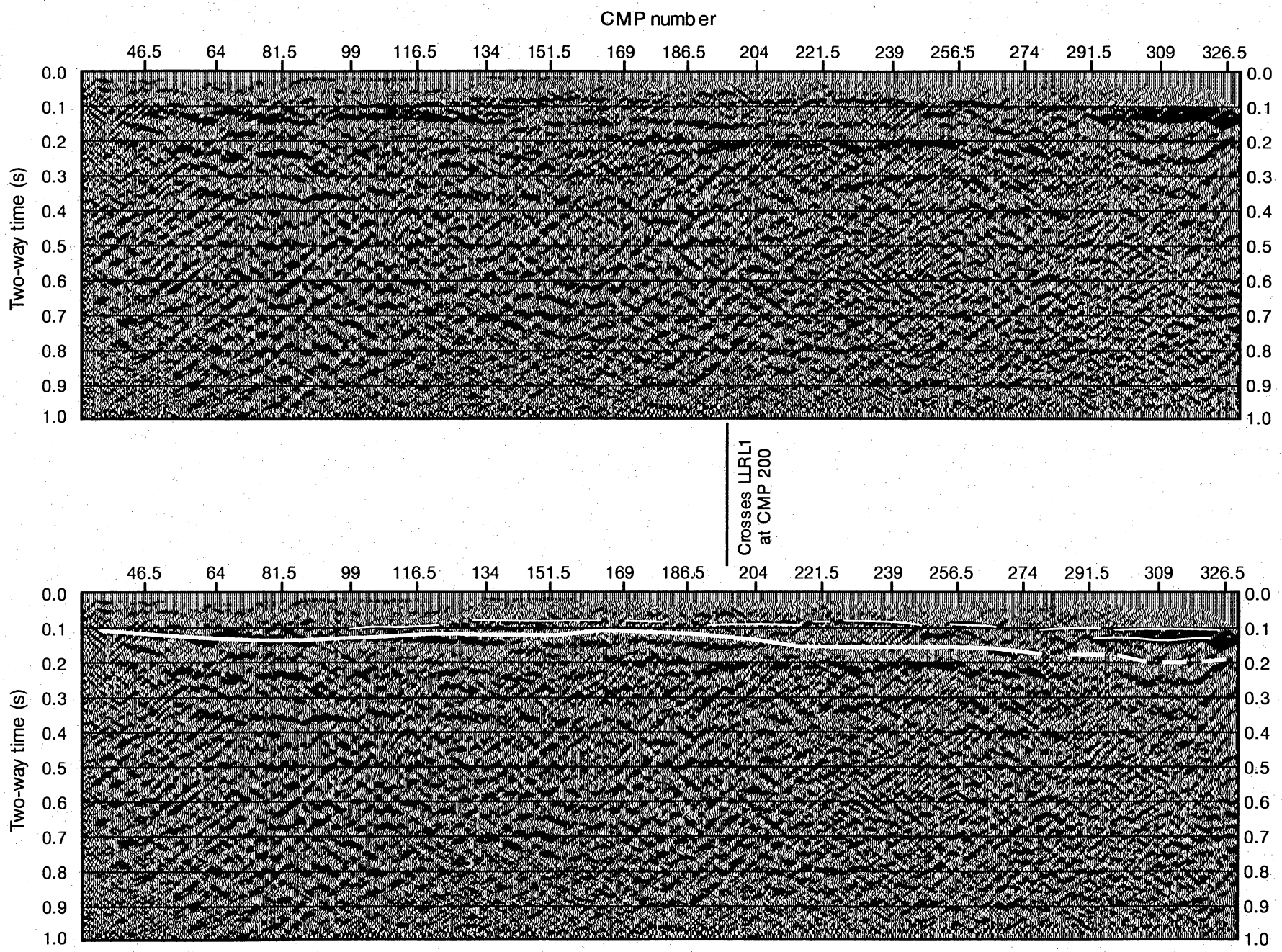

Figure 19. Faskin Ranch seismic reflection line LLRL2. Uninterpreted section at top; interpreted section at bottom. Heavy line represents interpreted bedrock reflector and lighter lines represent interpreted reflectors within the basin fill. Trace spacing 1.5 m. True amplitude display having automatic gain control applied. CMP locations shown in fig. 12.

segments can be seen within bedrock at several places along the line to about 350 ms. These reflectors appear to have little if any apparent dip.

Time-to-depth conversions show that the elevation at the interpreted top of bedrock decreases to the northeast from 4101 to 4182 ft (1250 to 1275 m) on the south half of the line to a minimum elevation of 3937 ft (1200 m) at the north end (fig. 20). Estimated basin-fill thickness (fig. 21) increases northward from 164 to 246 ft (50 to 75 m) to a maximum of 427 ft (130 m).

Line LLRL3

Line LLRL3, 4764 ft (1452 m) long, ties to line LLRL1 at CMP 207 (fig. 12). A high-amplitude reflector thought to be the bedrock reflector is present on the line between the south end and CMP 283 (fig. 22), but north of CMP 300 it becomes unclear. Lithologic control at borehole YM-17 near the north end of the line (fig. 12) allows a reflector to be picked at nearly 300 ms that can be tentatively carried southward and joined to the more certain pick on the south half of the line. Two-way time on this reflector increases from 125 ms at the south end to more than 200 ms near CMP 300 before increasing to 300 ms near YM-17. The reflector ties with the interpreted bedrock reflector on line LLRL1 at about 200 ms.

As on line LLRL1, interpreted basin-fill reflectors are present in the deeper part of the basin between about 100 and 250 ms and appear to onlap the bedrock surface as the bedrock reflector shallows to the south. Bedrock reflectors may be present to 300 ms, but little coherent energy is found deeper than that.

Depth conversions reveal that the elevation at the interpreted top of bedrock decreases from 4101 ft (1250 m) at the south end of the line to 3691 ft (1125 m) at the north end (fig. 23). Bedrock elevations appear to drop rapidly near CMP 300. Basin-fill thickness (fig. 24) increases northward along the line from 246 to 656 ft (75 to 200 m).

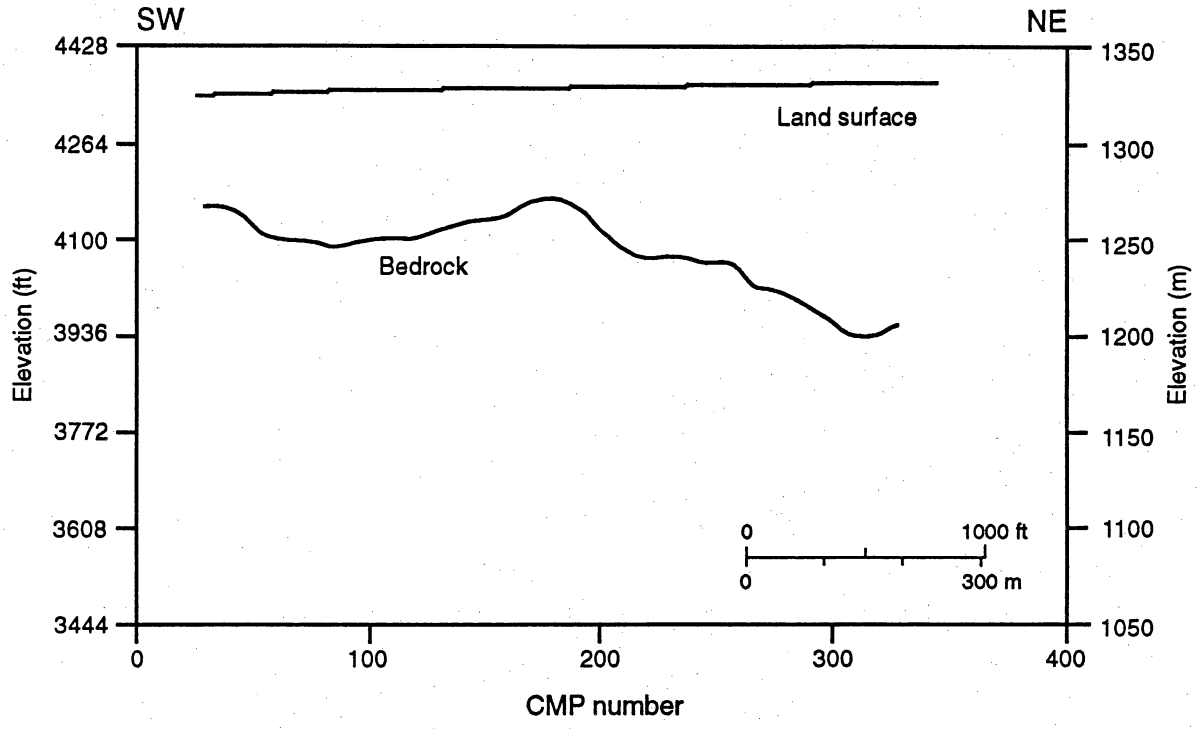

Figure 20. Land surface and estimated bedrock elevations of reflection line LLRL2. CMP locations shown in fig. 12. Vertical exaggeration = 2.5×.

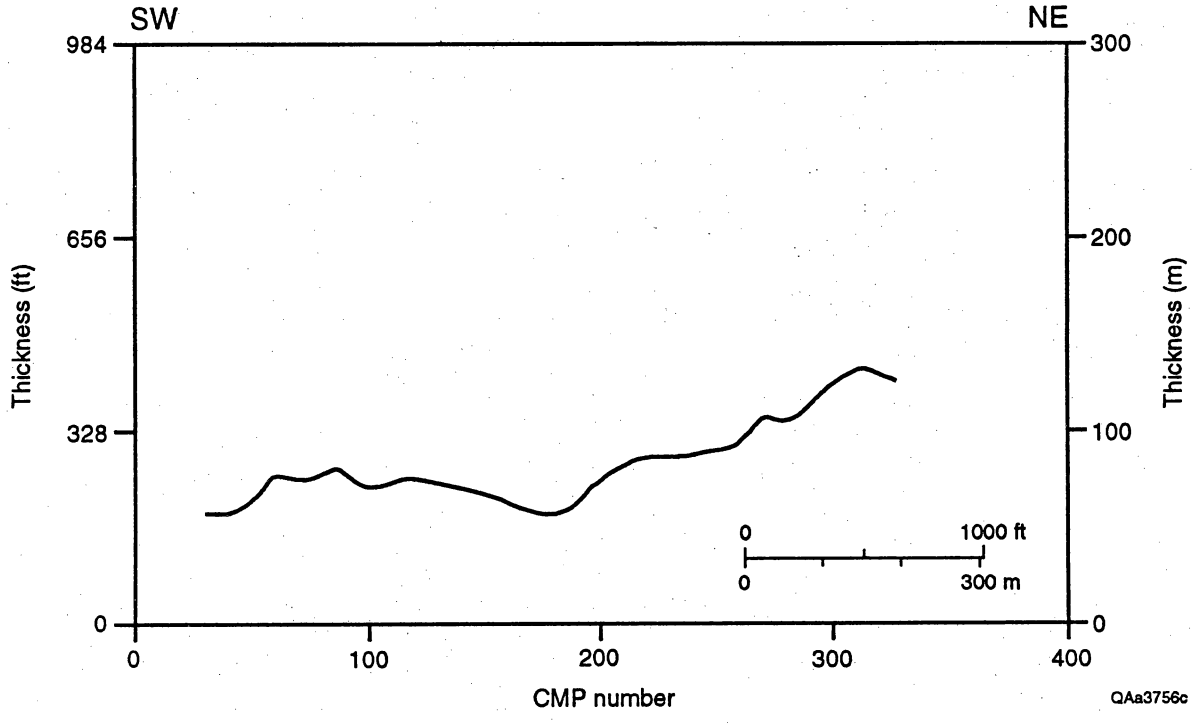

Figure 21. Estimated basin-fill thickness beneath reflection line LLRL2. CMP locations shown in fig. 12. Vertical exaggeration = 2.5×.

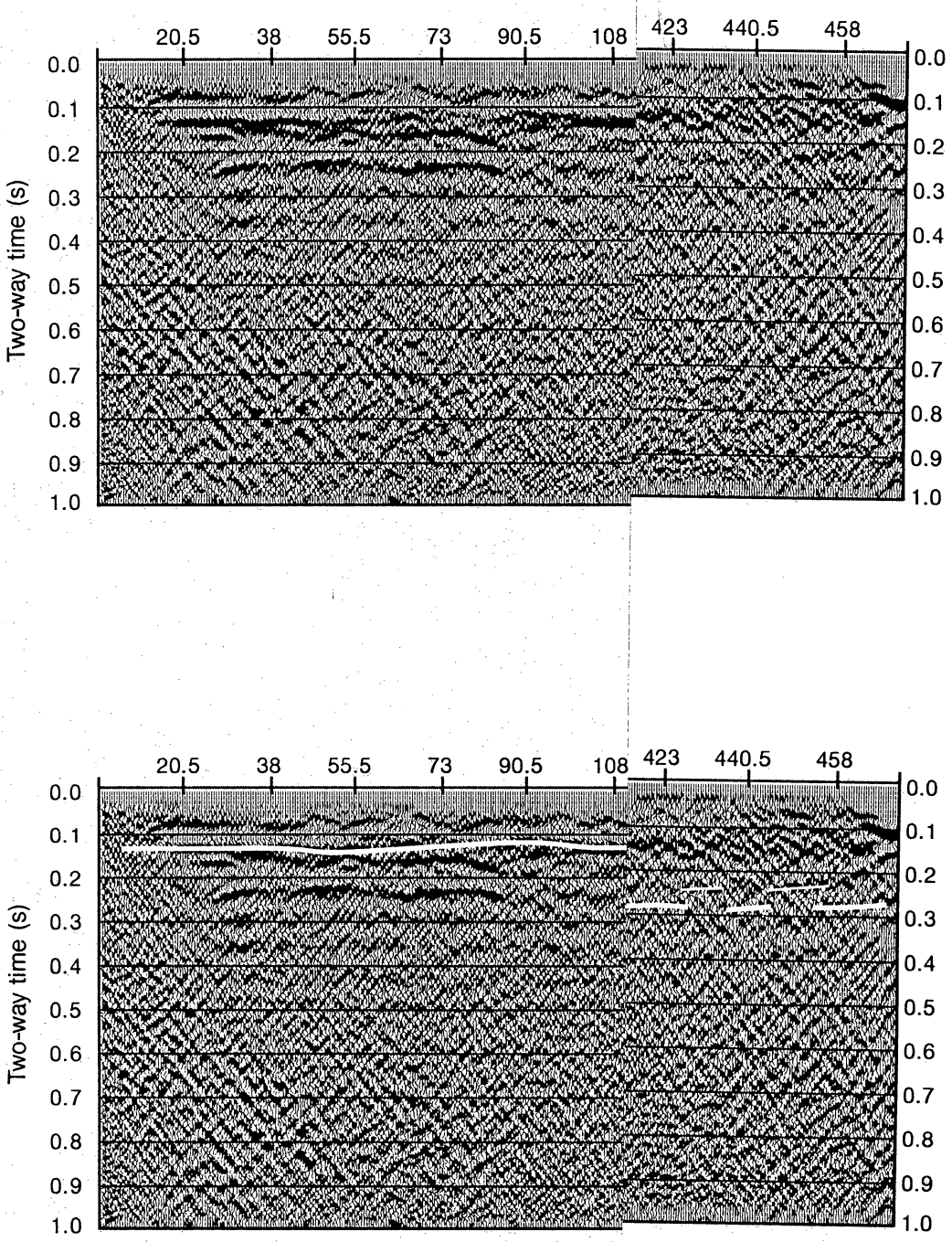

Figure 22. Faskin Ranch seismic reflection
interpreted section at bottom. Heavy line
lighter lines represent interpreted reflector
True amplitude display having automatic g
fig. 12.

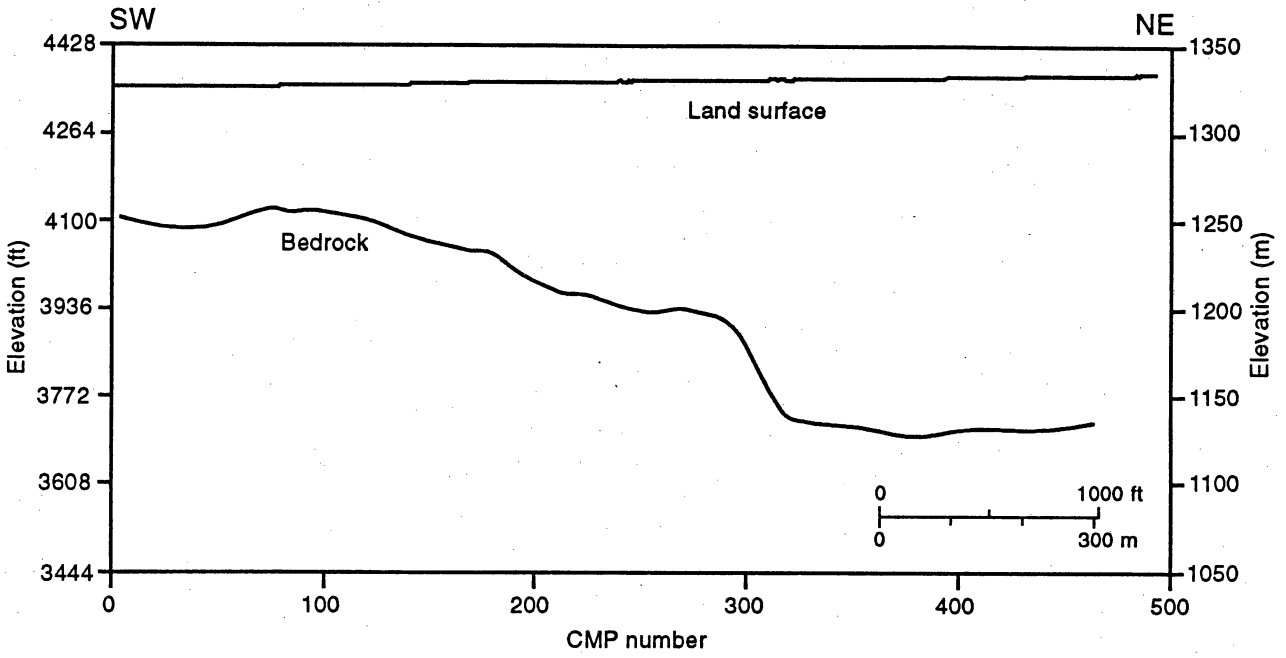

Figure 23. Land surface and estimated bedrock elevations of reflection line LLRL3. CMP locations shown in fig. 12. Vertical exaggeration = 2.5×.

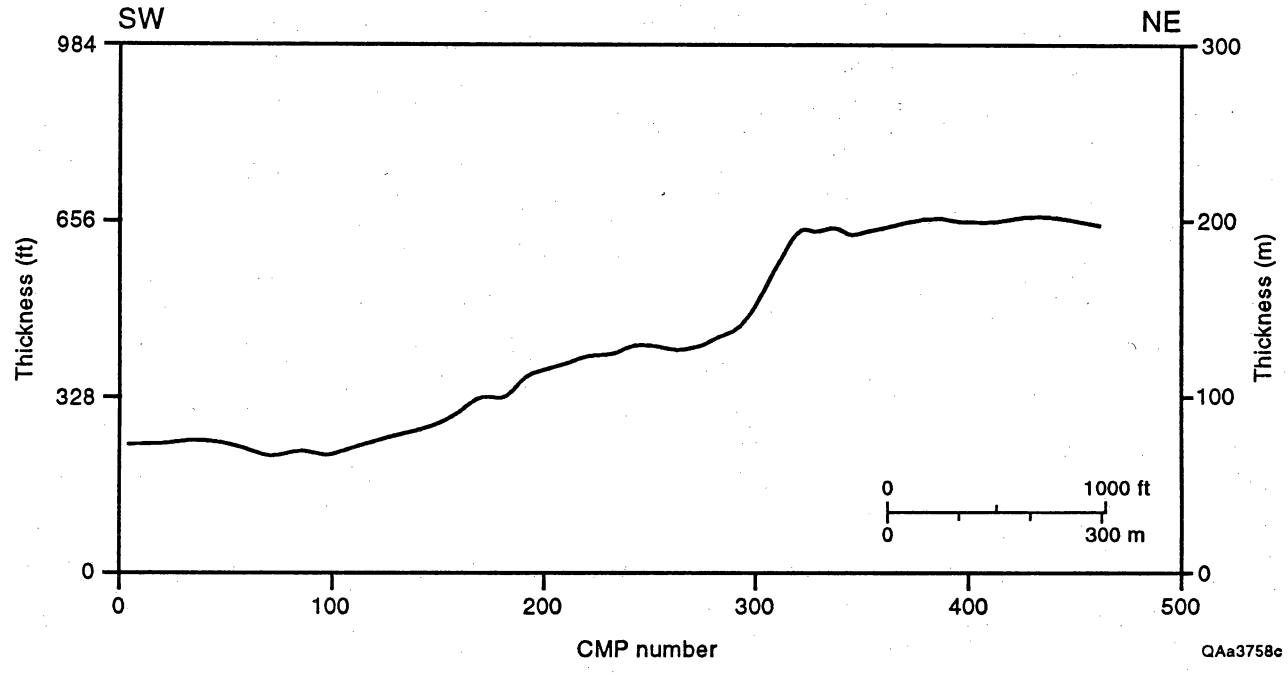

Figure 24. Estimated basin-fill thickness beneath reflection line LLRL3. CMP locations shown in fig. 12. Vertical exaggeration = 2.5×.

Line LLRL4

Reflection line LLRL4 ties to LLRL1 at CMP 193 and is 3871 ft (1180 m) long (fig. 12). Data quality along this line is the lowest of the four lines; consequently, bedrock elevations and estimates of basin-fill thickness are the most uncertain. Depth-to-bedrock control at borehole YM-63 near the north end of the line allowed selection of the reflector near 300 ms as the likely bedrock reflector (fig. 25). This reflector can be carried southward to the intersection with line LLRL1, where it ties with the bedrock reflector on that line just above 300 ms. Several reflectors could be the bedrock reflector south of the tie point, including the deepest one at 280 to 310 ms, a low-amplitude reflector at about 250 ms, a high-amplitude reflector at 150 to 200 ms, and a low amplitude reflector at about 100 ms. The deepest reflector appears to be the best selection from the seismic data alone, but would result in a depth to bedrock of nearly 656 ft (200 m) at the south end of the line. Only 1000 ft (300 m) away is borehole YM-5, where bedrock was reached at 164 ft (50 m). The best choice higher in the section is the high-amplitude reflector between 150 and 200 ms. If this horizon represents bedrock, the bedrock surface must deepen sharply between CMP's 250 and 200.

The deeper part of the basin at the north end of the line contains basin-fill reflectors between 150 and 250 ms. Bedrock reflectors are present as deep as 500 ms, below which little coherent energy exists.

Bedrock elevations calculated from two-way times (fig. 26) are tentatively interpreted near 4019 ft (1225 m) at the south end of the line and deepen rapidly in the center of the line to 3691 ft (1125 m). Estimated thickness of basin fill increases from 328 ft (100 m) on the south part of the line to 656 ft (200 m) on the north part (fig. 27).

Integration of Borehole and Seismic Data

Depths to bedrock determined from borehole and reflection seismic data at Faskin Ranch are in reasonable agreement (fig. 28). Seismic data indicate that the basin deepens to the

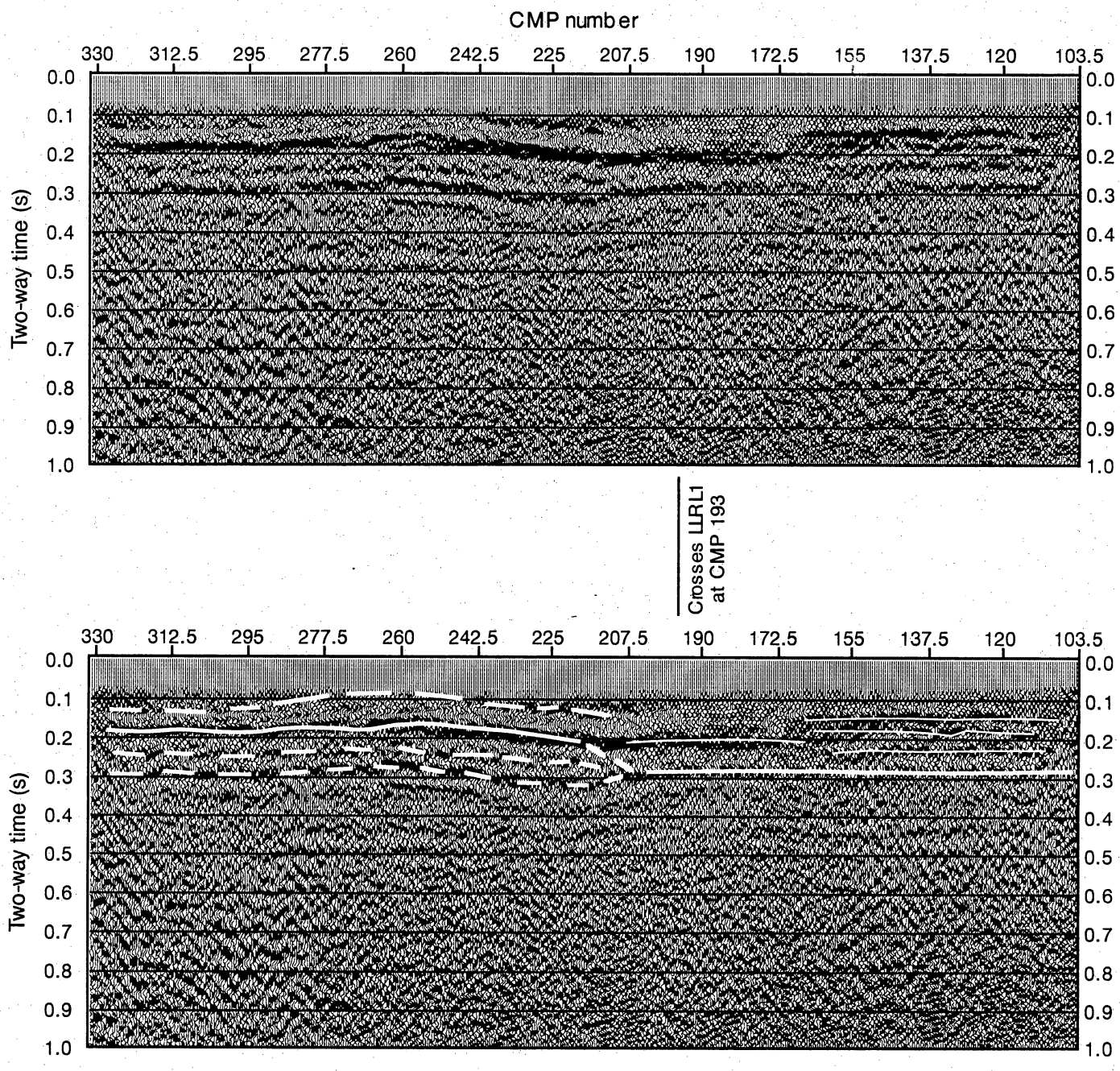

Figure 25. Faskin Ranch seismic reflection line LLRL4. Uninterpreted section at top; interpreted section at bottom. Heavy line represents interpreted bedrock reflector and lighter lines represent interpreted reflectors within the basin fill. Dashed heavy lines represent alternate bedrock interpretations. Trace spacing 2.5 m. True amplitude display having automatic gain control applied. CMP locations shown in fig. 12.

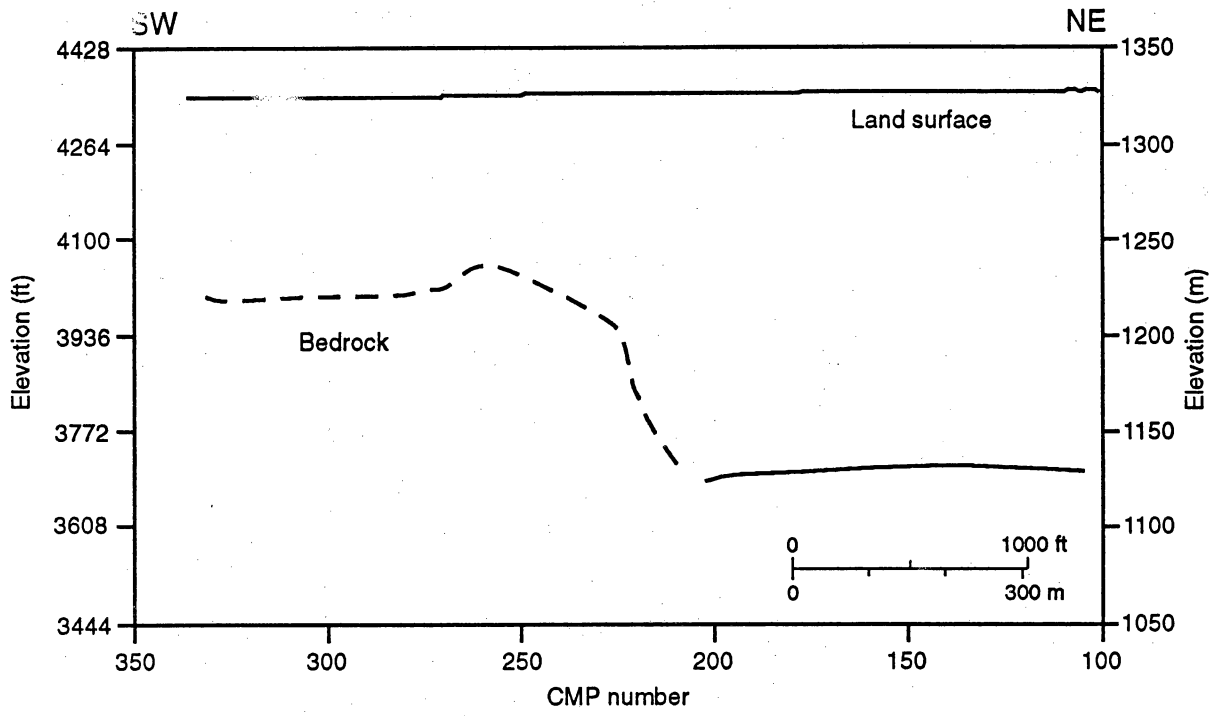

Figure 26. Land surface and estimated bedrock elevations of reflection line LLRL4. CMP locations shown in fig. 12. Vertical exaggeration = 2.5×.

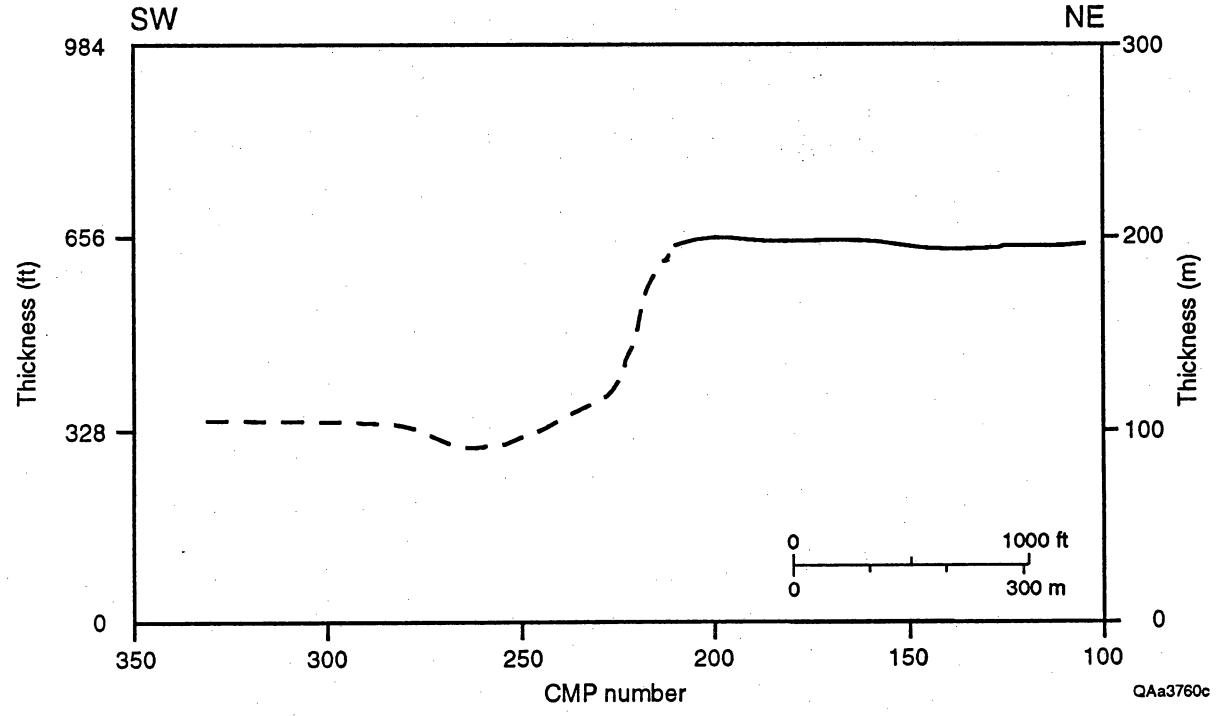

Figure 27. Estimated basin-fill thickness beneath reflection line LLRL4. CMP locations shown in fig. 12. Vertical exaggeration = 2.5×.

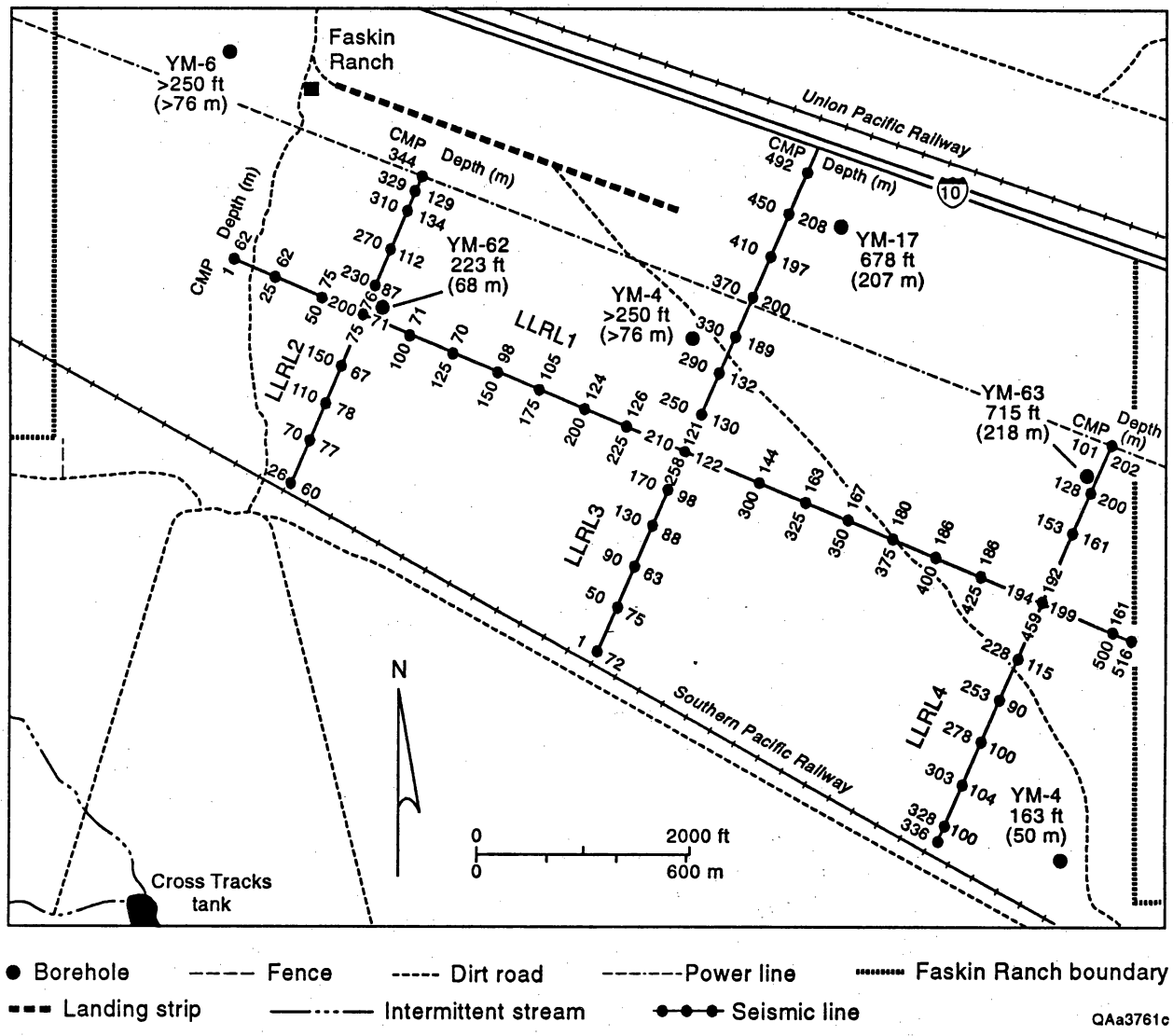

Figure 28. Depth-to-bedrock estimates from seismic reflection lines LLRL1, LLRL2, LLRL3, and LLRL4. Also shown are depths to bedrock in nearby boreholes.

southeast along line LLRL1 and to the northeast along each of the three crossing seismic lines. Similarly, existing boreholes that reach bedrock (YM-5, YM-17, YM-62, and YM-63) indicate bedrock depths increase north of line LLRL1. Primary lithologic control on line LLRL1 is provided by borehole YM-62, which reached bedrock at 223 ft (68 m). Estimated bedrock depth on line LLRL1 near this site is 234 to 249 ft (71 to 76 m). No other boreholes were drilled near this line. Secondary control on LLRL1 bedrock depths is provided at its intersection with line LLRL4, where the bedrock reflector is tied to a bedrock depth in borehole YM-63. Control of the bedrock reflector on line LLRL2 is also provided by borehole YM-62; bedrock depth at the borehole (223 ft [68 m]) is estimated at 233 ft (71 m) on LLRL2.

Two boreholes lie near line LLRL3. Borehole YM-4, near CMP 290, was drilled to 250 ft (76 m) and did not reach bedrock. Estimated bedrock depths in this area are 427 to 623 ft (130 to 190 m), values that are consistent with drilling results. Bedrock was reached at YM-17 at 679 ft (207 m), in agreement with nearby estimated depths of 646 to 682 ft (197 to 208 m). No borehole control exists on the south half of line LLRL3.

Control on line LLRL4 is provided by borehole YM-63, which was drilled near the north end of the line. Bedrock in the borehole (715 ft [218 m] deep) is deeper than bedrock estimated from the seismic line (656 ft [200 m]), but the velocity function used to stack the section is slightly higher than the function used to convert two-way times to depth. A higher conversion velocity would decrease the magnitude of the depth discrepancy. Bedrock depths estimated from seismic data at the south end of LLRL4 do not agree closely with the bedrock depth found in nearby borehole YM-5. It is unknown whether the depth inferred from the seismic data is real or whether the seismic data are interpreted improperly in this area.

Reflection lines LLRL1, LLRL3, and LLRL4 and boreholes YM-17 and YM-63 all indicate that the basin deepens in the northeast part of the study area. The deep basin floor has an elevation near 3691 ft (1125 m); this elevation appears to rise sharply to the south. The south boundary of the deep basin floor has a southeasterly trend and probably crosses LLRL4

between CMP's 194 and 228, LLRL1 between CMP's 375 and 400, and LLRL3 between CMP's 290 and 330. The boundary apparently passes north of line LLRL2.

Surface Wave Analysis

The seismic work at Faskin Ranch included a study on the feasibility of using surface waves (ground roll) to generate shear-wave-velocity models of the shallow subsurface. A limited seismic experiment was conducted using acquisition parameters optimized for surface wave recording. Shot records from the seismic reflection and refraction data acquired at the site were also analyzed for surface waves. This section of the report explains the basic principles behind surface wave analysis to find subsurface velocity and presents preliminary results from the Faskin Ranch work.

Introduction

The dispersiveness of seismic surface waves is commonly used to constrain the velocity structure of the earth. Dispersion of seismic waves occurs if different seismic wavelengths travel at different velocities. Rock velocity generally increases with depth in the earth. For dispersive waves, this means that longer wavelengths travel faster than shorter wavelengths because longer wavelengths sample the faster rocks deeper in the earth. By measuring phase velocity as a function of wavelength in surface waves, one can obtain true rock velocity from the data through an inversion procedure (for example, Kovach, 1978; Aki and Richard, 1980).

In this analysis, phase velocity estimates were obtained using the Fourier phase method (Sato, 1955, 1956). In this procedure, one analyzes the phase curve obtained by taking the difference between two seismograms from the same shot record in the Fourier domain. An equivalent procedure is to take the difference between seismograms from different shot locations recorded by the same receiver. At a given frequency, the phase value represents the phase shift due to the difference in source–receiver distance for each seismogram. In the case

of constant velocity, the unwrapped phase curve is a straight line because all frequencies in the data see the same velocity material. In cases where rock velocity varies with depth, the phase curves will deviate from a straight line. Higher frequencies will sense the shallow velocity structure, whereas lower frequencies will sense deeper velocity structure.

The phase velocity can be obtained from the phase curves from the relationships

$$\Phi/360 = d/\lambda, \text{ and} \quad (1)$$

$$c = f\lambda, \quad (2)$$

where Φ is the phase in degrees, d is the distance between the geophones that recorded the seismograms, λ is the wavelength, f is frequency, and c is phase velocity. Given a phase curve, equation 1 is solved for wavelength (λ), and the phase velocity is obtained from equation 2. An approximate conversion from phase velocity and wavelength to rock velocity and depth is obtained by assuming that the observed phase velocity represents the shear velocity at a depth equal to one-third to one-half the wavelength.

An accurate mapping of phase velocity and wavelength to shear velocity and depth is obtained through modeling or inversion schemes. In this study, the inversion method of Yuan (1992) was used to obtain preliminary shear-velocity models from the surface waves. An important assumption underlying this analysis is that the data contain only Rayleigh waves and no other modes.

Data

Receiver gathers from the surface wave experiment are found in figure 29 and some of the better quality raw phase curves from the surface wave experiment are in figures 30 and 31. Synthetic phase curve for each separation, assuming a phase velocity of 1312 ft/s (400 m/s) is included in the figures as a guide to data quality. These data are most reliable at 66- and 131-ft (20- and 40-m) separations near the geophones. Data quality deteriorates at large distances from the geophones and at larger separations. In pavement applications, phase data are most reliable

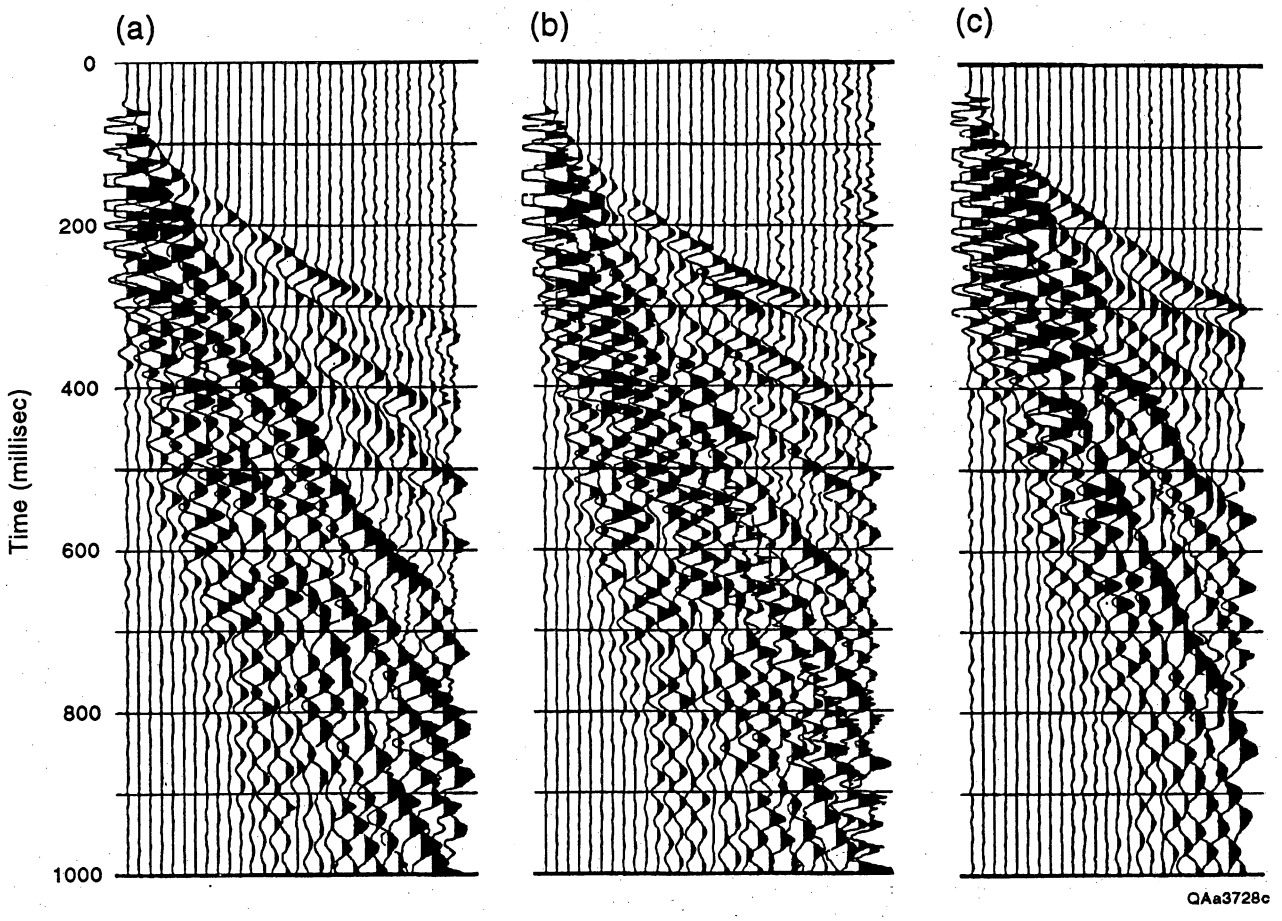

Figure 29. Field records of surface wave experiment. (a) Records of 8-Hz phone from westward-moving source. (b) Stacked records of 40-Hz phones from westward-moving source. (c) Records of 8-Hz phone from eastward-moving source. 40-Hz phones did not record eastward-moving source.

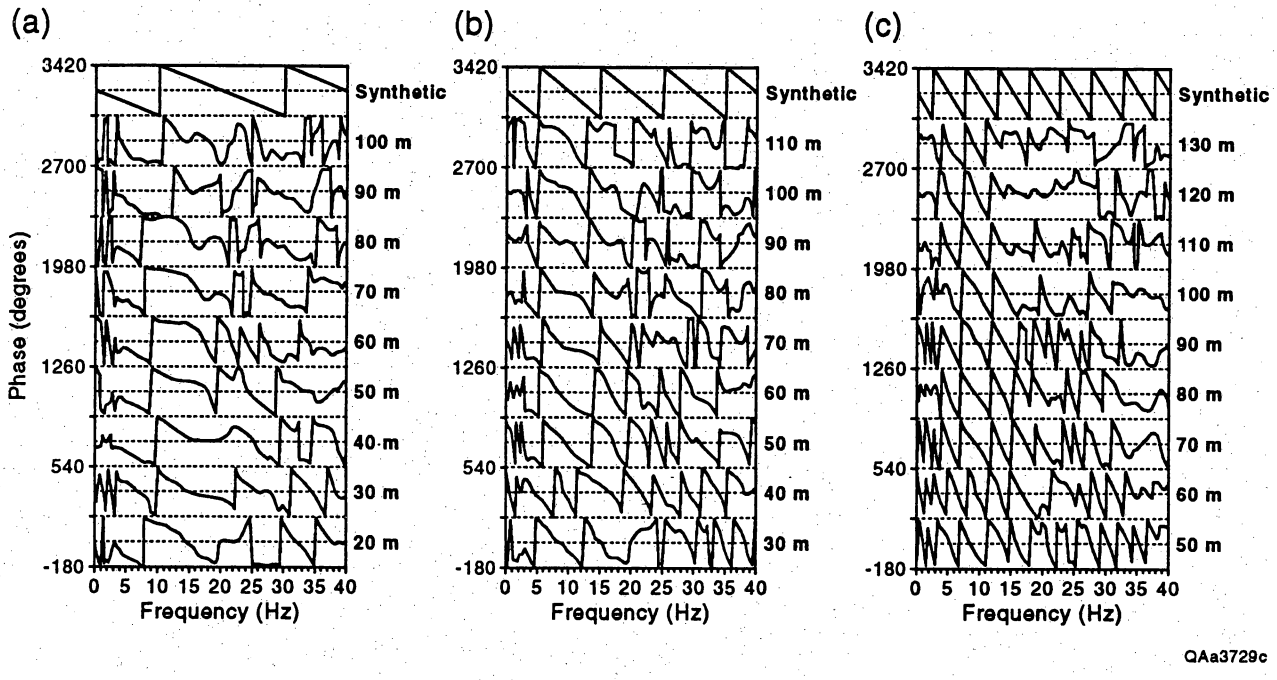

Figure 30. Raw phase curves of 8-Hz records of westward-moving source. Curves of (a) 20-, (b) 40-, and (c) 80-m source separation shown along with a synthetic curve that assumes a constant phase velocity of 400 m/s. Distance from source to geophones is annotated on right-hand side of graphs.

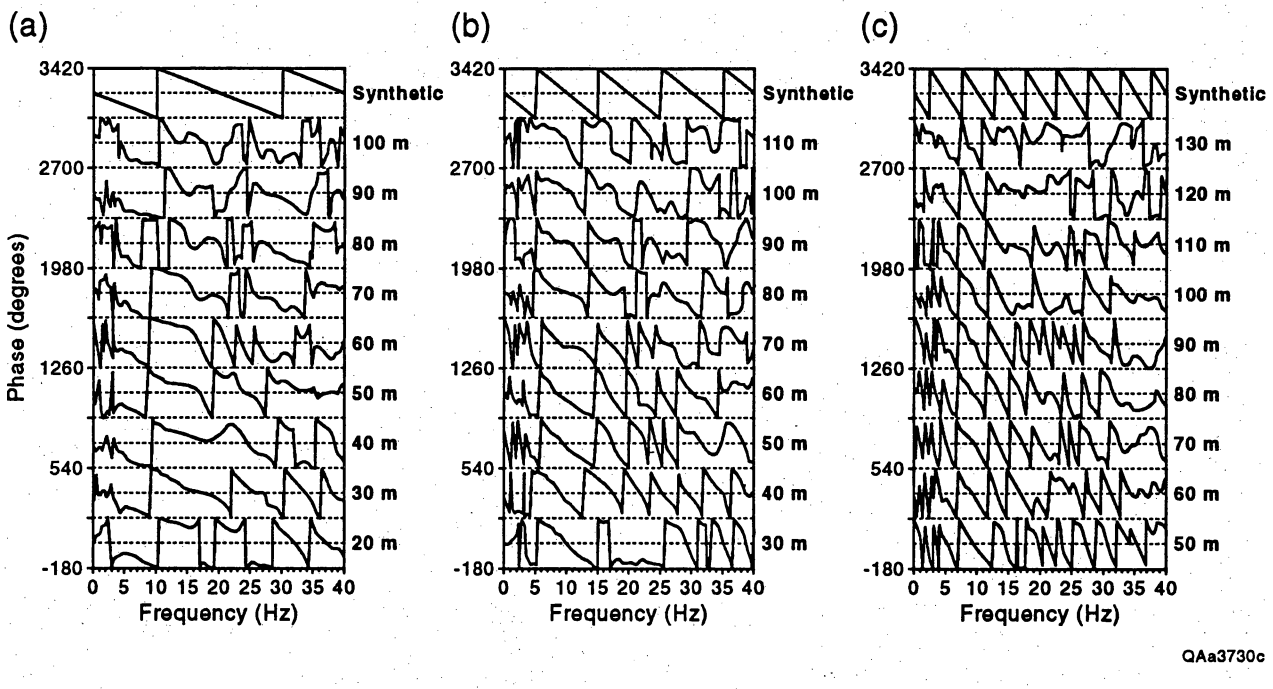

Figure 31. Raw phase curves of 40-Hz records of westward-moving source. Curves of (a) 20-, (b) 40-, and (c) 80-m source separation shown along with a synthetic curve that assumes a constant phase velocity of 400 m/s. Distance from source to geophones is annotated on right-hand side of graphs.

over the first two cycles of the phase curves (0 to 720). This is probably a useful guide for these data as well. Thus phase curves that are inconsistent in this range represent poor data.

Because a key to accurately estimating phase velocity is good phase data at low frequencies, the surface wave experiment was conducted using an 8-Hz geophone and a 4-Hz low cut in the acquisition system. An unanticipated result from the experiment is that the phase curves of the 8-Hz and 40-Hz phones are virtually identical, which suggests that the acquisition system has enough dynamic range that the lower-resonance frequency phone is unnecessary for good recording. Plots of amplitude (fig. 32) of the two different phone types bear this out. This result should be an asset in future surface wave studies using shallow seismic reflection equipment because it shows that surface wave data can be collected using the higher-resonance frequency geophones that are commonly used in such surveys.

As expected, analysis of shot gathers from the seismic reflection survey showed that the low-cut filter used during acquisition affects surface-wave data quality. Both 16- and 32-Hz low-cut filters were used for the acquisition of the reflection data. Phase curves generated from these data (fig. 33) were of very poor quality. Comparison of amplitude spectra of a 4-Hz and a 16-Hz low cut (fig. 34) shows that at frequencies below 16 Hz, trace amplitudes were 60 dB down, compared with the data from the surface wave experiment. Because high low-cut filters are commonly used in shallow reflection surveys to attenuate surface waves during acquisition, this result is not surprising.

Data Processing Procedures

The basic steps for obtaining shear-velocity information from surface waves are: (1) calculating raw phase curves, (2) phase curve unwrapping and smoothing, (3) calculating phase velocity and wavelength, and (4) inverting for shear velocity and depth.

Obtaining good phase-velocity results from the phase curves requires that they be fit to an expected curve. A Kalman filter was used to perform this task on these data. Figure 35 shows an

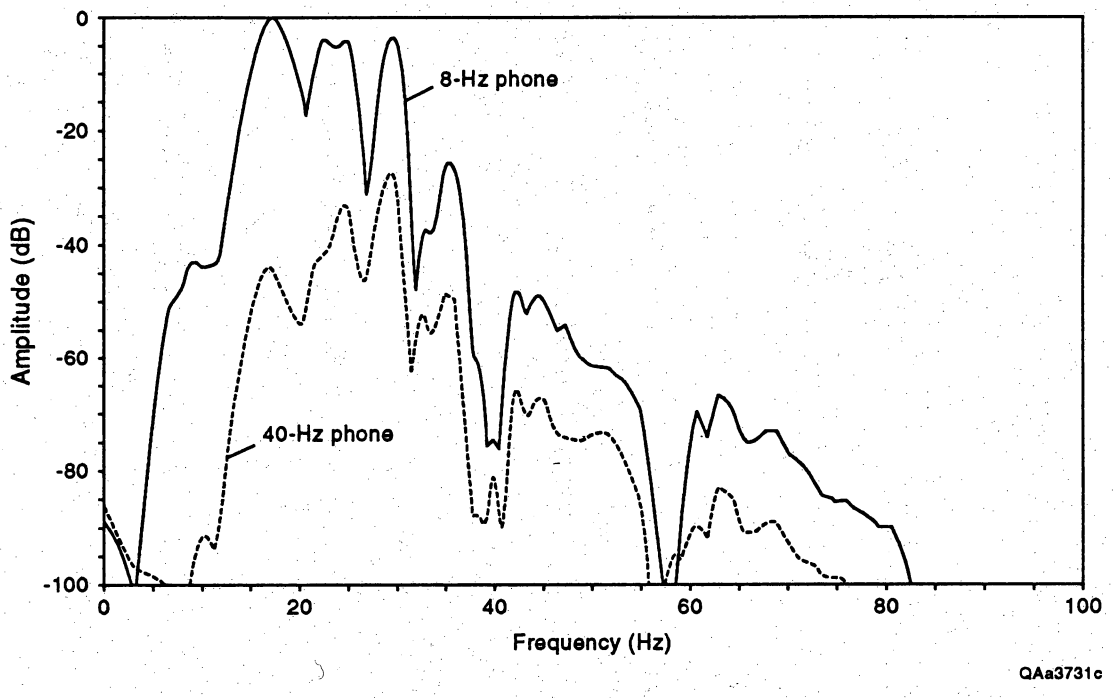

Figure 32. Amplitude spectra of 8-Hz and 40-Hz phones at 50-m offset of the westward-moving source.

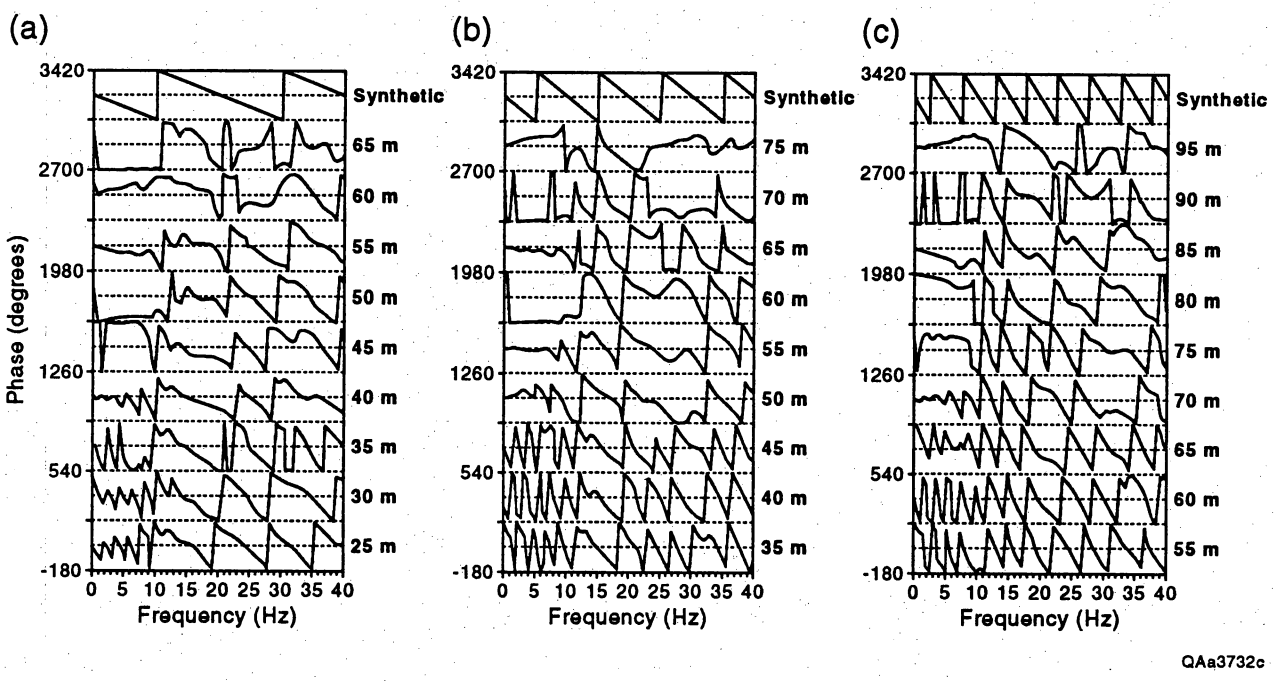

Figure 33. Raw phase curves from a shot gather from reflection profile LLFR-1. Curves of (a) 20-, (b) 40-, and (c) 80-m source separation are shown along with a synthetic curve that assumes a constant phase velocity of 400 m/s. Distance from source to geophones is annotated on right-hand side of graphs.

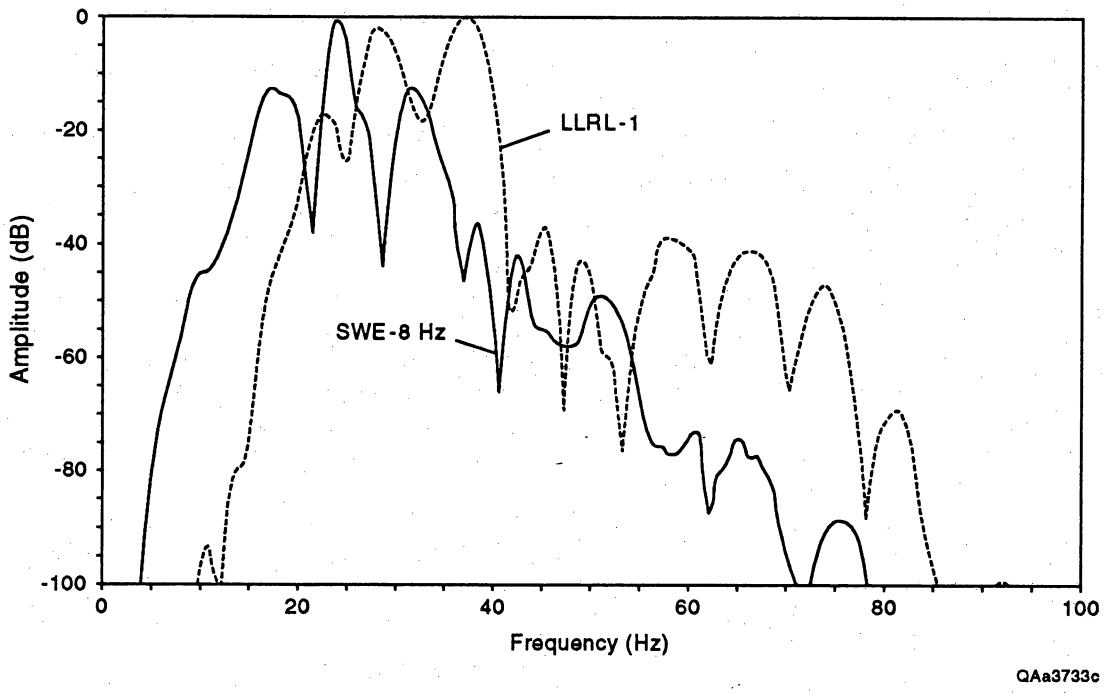

Figure 34. Amplitude spectrum of reflection data (LLRL1) compared with surface-wave data (SWE) from west-moving source.

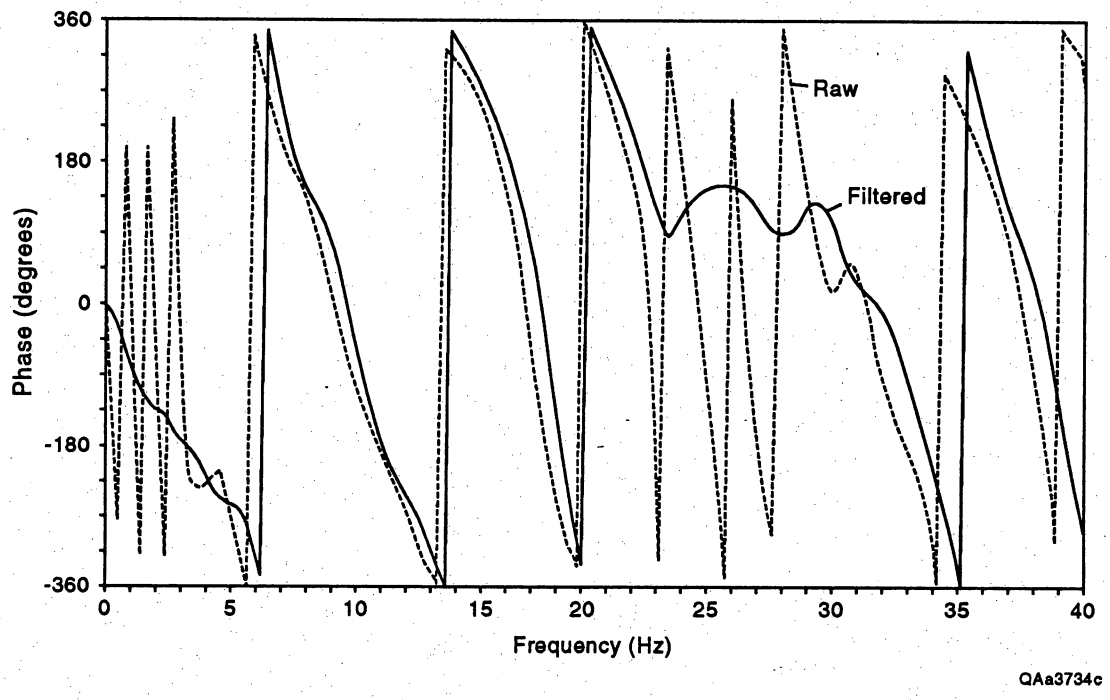

Figure 35. Example of Kalman filter fit.

example of a raw phase curve and the filtered curve. The primary effect of the Kalman filter is the definition of a smooth expected curve for the low-frequency end of the phase spectrum, in order to achieve stable phase-velocity results. Kalman filtering is less effective in larger separations because phase curves may wrap more than once in the poor data zone at low frequencies.

Phase velocity and wavelength are calculated from the filtered phase curves using the equations cited above. These data are most reliable on wavelengths between one-half and twice the separation. Figure 36 shows curves from three separations at three different locations in the surface wave experiment. The center points of each of these separate graphs are only 32.8 ft (10 m) apart. Note that the 66- and 131-ft (20- and 40-m) curves are consistent from location to location, but the 263-ft (80-m) curve is not. This probably results from poor data quality at the low frequencies in the larger separation.

A one-dimensional model of shear velocity as a function of depth is obtained through inversion of the phase velocity information. The curves of all separations at a given site are fit with a single curve (fig. 37) that is then input to the inversion scheme. Two alternative velocity models of sites are shown in figure 38. The corresponding fit to the input phase velocity curve is shown in figure 39.

CONCLUSIONS

Seismic refraction, reflection, and surface wave data collected at the proposed low-level radioactive waste disposal site on Faskin Ranch varied in quality but revealed much about basin geometry and the physical properties of basin-fill sediments. Refraction data indicate that near-surface seismic velocities range from 1243 to 1447 ft/s (379 to 441 m/s) and that velocities of the underlying basin-fill layer range from 3110 to 3628 ft/s (948 to 1106 m/s). A refracted arrival from bedrock was recorded at most refraction sites, but a limited offset range precluded velocity measurements accurate enough to calculate depth to bedrock reliably at every site.

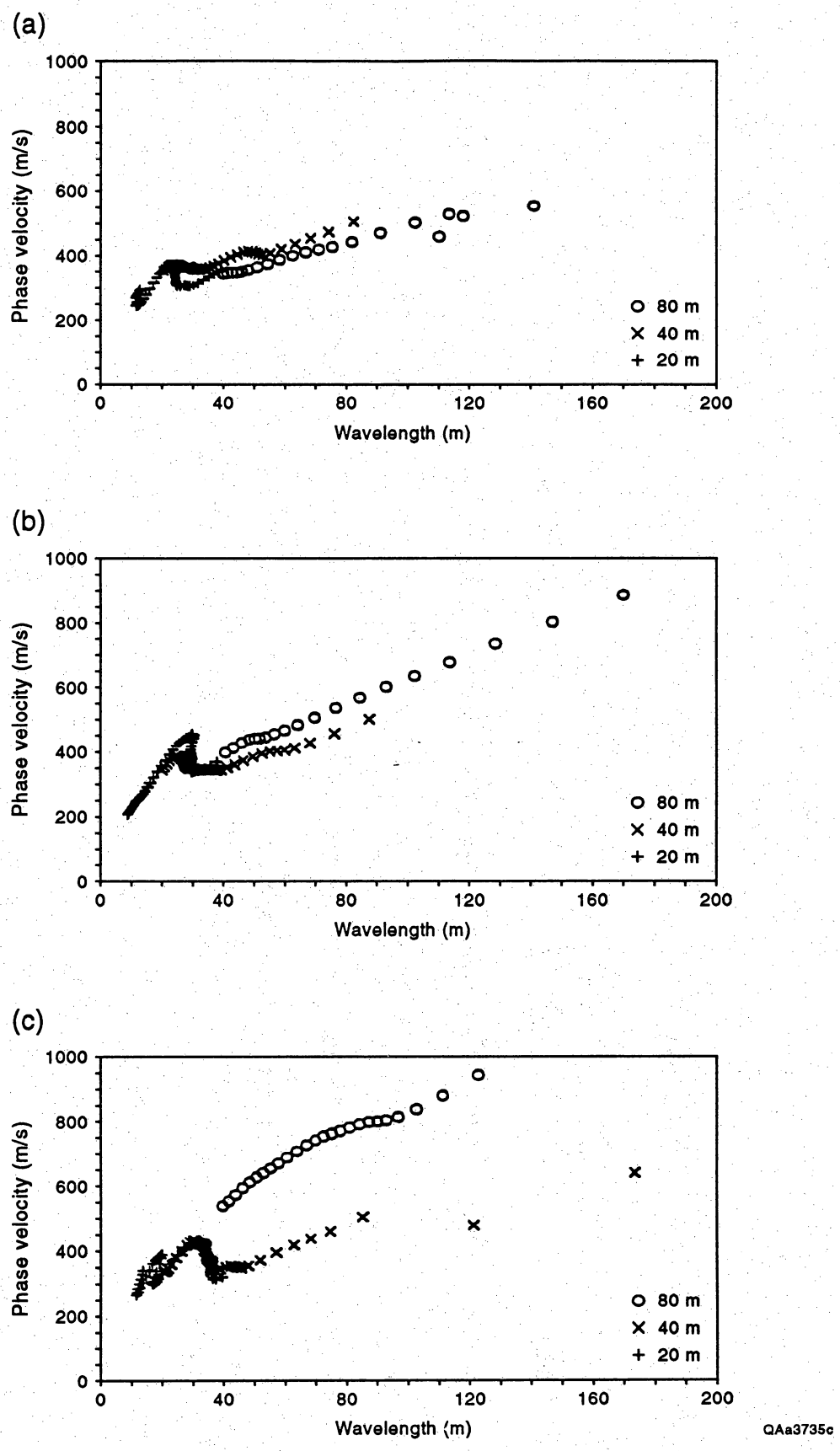

Figure 36. Phase velocity curves of (a) 50-m center point, westward-moving source; (b) 60-m center point, westward-moving source; and (c) 70-m center point, westward-moving source.

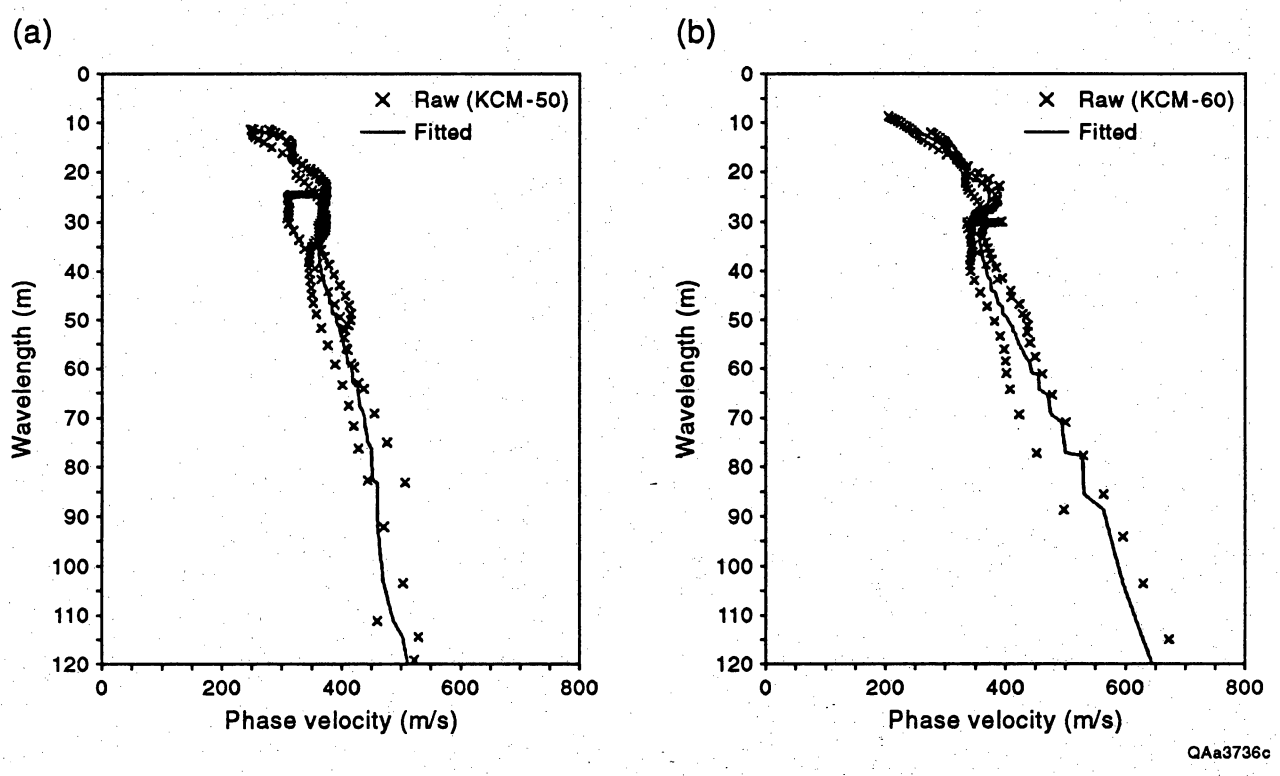

Figure 37. Curve fits of input to inversion: (a) 50-m center point, westward-moving source; and (b) 60-m center point, westward-moving source.

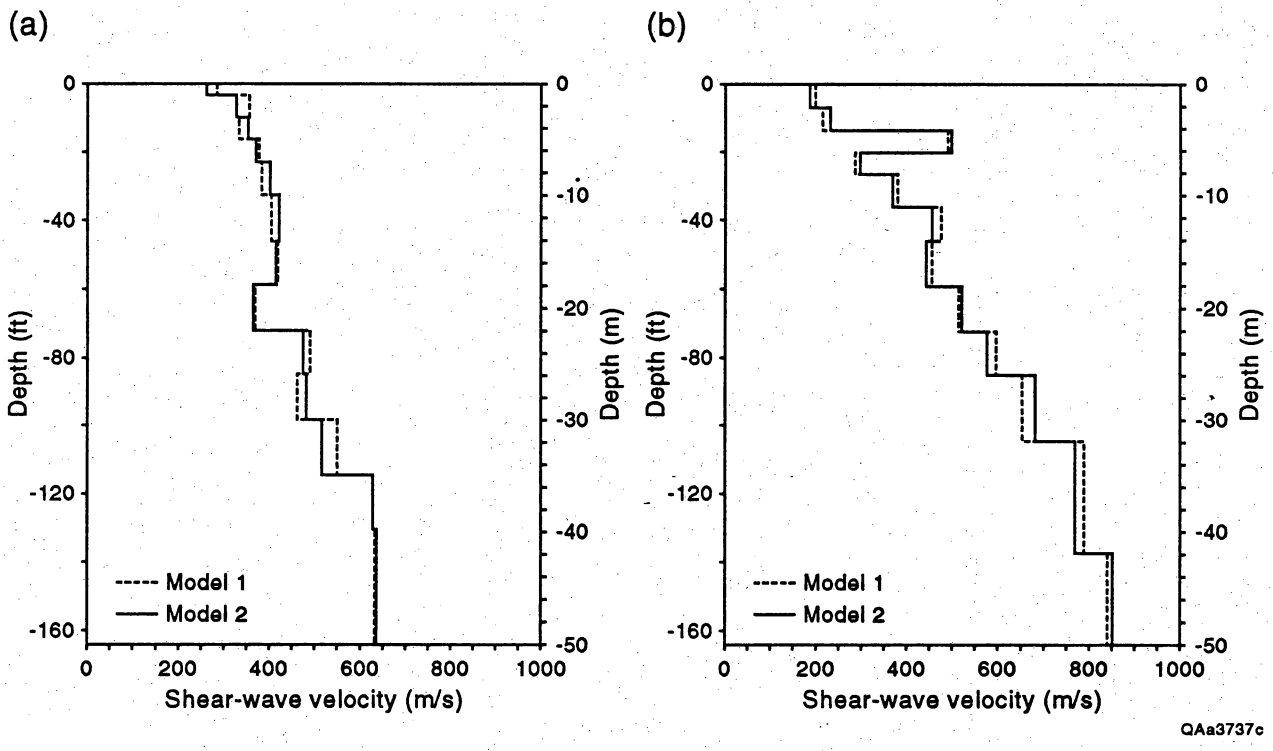

Figure 38. Inversion models: (a) 50-m center point, westward-moving source, and (b) 60-m center point, westward-moving source.

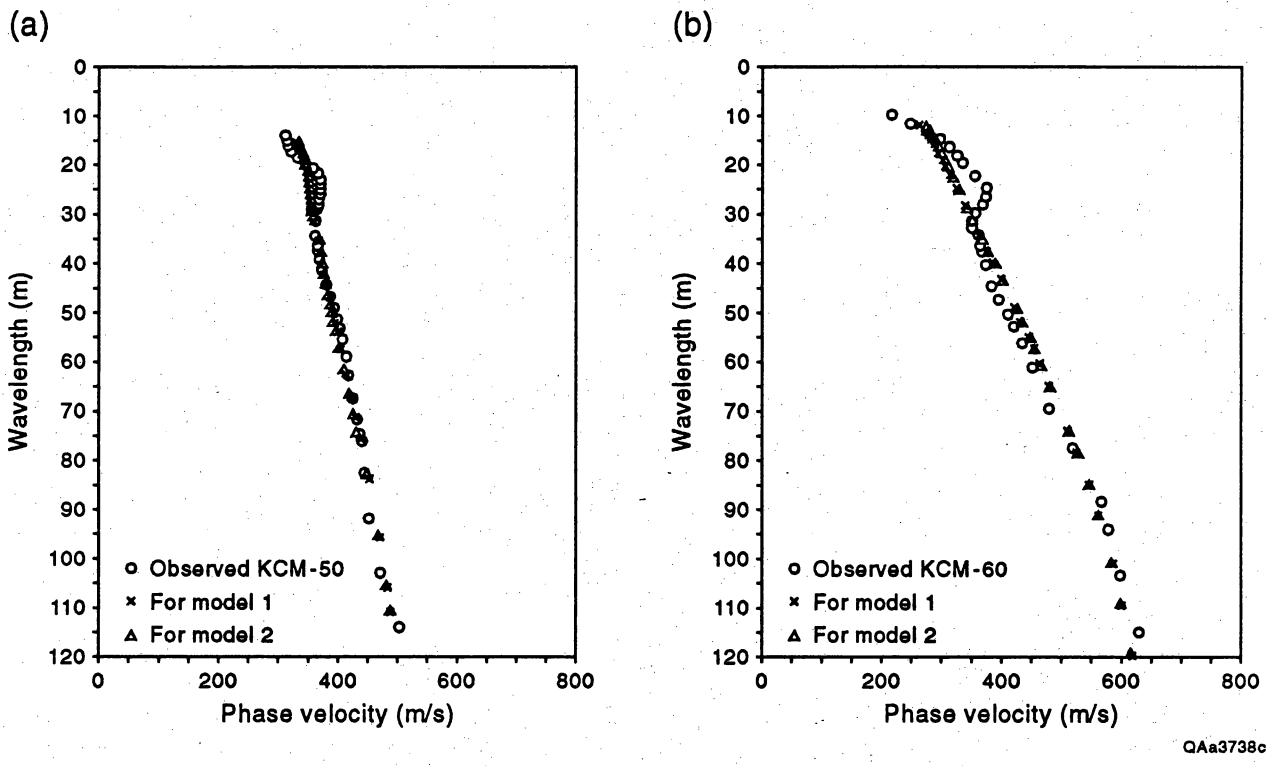

Figure 39. Fit of phase velocity predicted from inversion to original data: (a) 50-m center point, westward-moving source, and (b) 60-m center point, westward-moving source.

A borehole velocity survey at well YM-63 showed that seismic velocities increase rapidly from 1312 to 2625 ft/s (400 to 800 m/s) in the upper 33 ft (10 m) of basin fill. Below this depth, average velocities continue to increase at a slower rate and reach 3281 ft/s (1000 m/s) by a depth of 194 ft (59 m). Extrapolations to deeper depths from borehole velocity data provided useful velocity functions in seismic data processing.

Four shallow seismic reflection lines were collected over a distance of 3.9 mi (6.2 km) at the site. Bedrock deeper than expected and difficult site conditions reduced data quality on the initial lines, but changes in acquisition geometry improved bedrock imaging on the longest of the lines. An interpreted bedrock reflector is visible in stacked sections in most areas; internal basin-fill reflectors are also present in the deeper parts of the basin. Reflectors below the top of bedrock are evident in some areas. Depths to bedrock estimated from seismic data range from about 197 ft (~60 m) to more than 656 ft (>200 m) and increase to the north and east on all lines. The deepest section of the basin is present in the northeast part of the site and is separated from shallower parts of the basin by a relatively abrupt and steeply dipping boundary.

A feasibility study on using surface waves (ground roll) to generate shear-wave-velocity models of the shallow subsurface was conducted at Faskin Ranch. A preliminary one-dimensional velocity model of a site near the intersection of reflection lines LLRL1 and LLRL3 was found. This result provides velocity data on the upper few tens of meters for which little data in seismic reflection survey exist. If future surface waves studies are done, we recommend that:

1. Surface wave data be collected during the course of a reflection survey by reducing the low cut on the field filters periodically. Results from the Faskin Ranch survey suggest that a 40-Hz geophone can do a good job collecting the low end of the frequency spectrum.

2. In production mode, a field quality control system be designed that can plot phase curves, real time, so that data quality can be checked.

3. Other wave packets be removed from the data, by trace muting, for example, to improve phase curve quality. Surface wave analysis assumes that the trace represents a record of Rayleigh waves only. If other wave modes are present, data quality is degraded.

4. The shear-velocity data collected from surface wave analysis be used in combination with compressional wave data on velocity to characterize lithology through analysis for Poisson's ratio.

ACKNOWLEDGMENTS

We wish to thank the staff of the Sierra Blanca office of the Texas Low-Level Radioactive Waste Disposal Authority for their logistical support during seismic data acquisition. Appreciation for technical support is extended to Allan Standen, Bart Kelley, Tom Jones, and Steve Rooks. Illustrations were prepared by Kerza A. Prewitt and Susan Krepps under the direction of Richard L. Dillon. This report was reviewed by Steven J. Seni, word processed by Susan Lloyd, and edited by Lana Dieterich. Jamie H. Coggin assembled the report, and Tucker F. Hentz was the technical editor.

REFERENCES

Aki, Keitti, and Richards, P. G., 1980, Quantitative seismology: theory and methods: San Francisco, W. H. Freeman and Company, 932 p.

Kovach, R. L., 1978, Seismic surface waves and crustal and upper mantle structure: Reviews of Geophysics and Space Physics, v. 16, p. 1–13.

Mayne, W. H., 1962, Common reflection point horizontal data stacking techniques: Geophysics, v. 27, p. 927–938.

Milsom, John, 1989, Field geophysics: London, Open University Press, Milton Keynes, Geological Society of London Handbook, 182 p.

Palmer, Derecke, 1986, Refraction seismics: the lateral resolution of structure and seismic velocity, *in* Helbig, Klaus, and Treitel, Sven, eds., Seismic exploration: London, Geophysical Press, Handbook of Geophysical Exploration, v. 13, 269 p.

Sato, Y., 1955, Analysis of dispersed surface waves by means of Fourier transform, 1: Bulletin of the Earthquake Research Institute, University of Tokyo, v. 33, p. 33–47.

Sato, Y., 1956, Analysis of dispersed surface waves by means of Fourier transform, 2: synthesis of movement near the origin: Bulletin of the Earthquake Research Institute, University of Tokyo, v. 34, p. 9–18.

Steeples, D. W., and Miller, R. D., 1990, Seismic reflection methods applied to engineering, environmental, and groundwater problems, *in* Ward, S. H., ed., Geotechnical and environmental geophysics: Tulsa, Oklahoma, Society of Exploration Geophysicists, Investigations in Geophysics No. 5, v. 1, p. 1–30.

Yilmaz, Ozdogan, 1987, Seismic data processing: Tulsa, Oklahoma, Society of Exploration Geophysicists, Investigations in Geophysics No. 2, 526 p.

Yuan, D., 1992, Some aspects of the inversion problem of surface wave dispersion data: The University of Texas at El Paso, Ph.D. dissertation, 150 p.